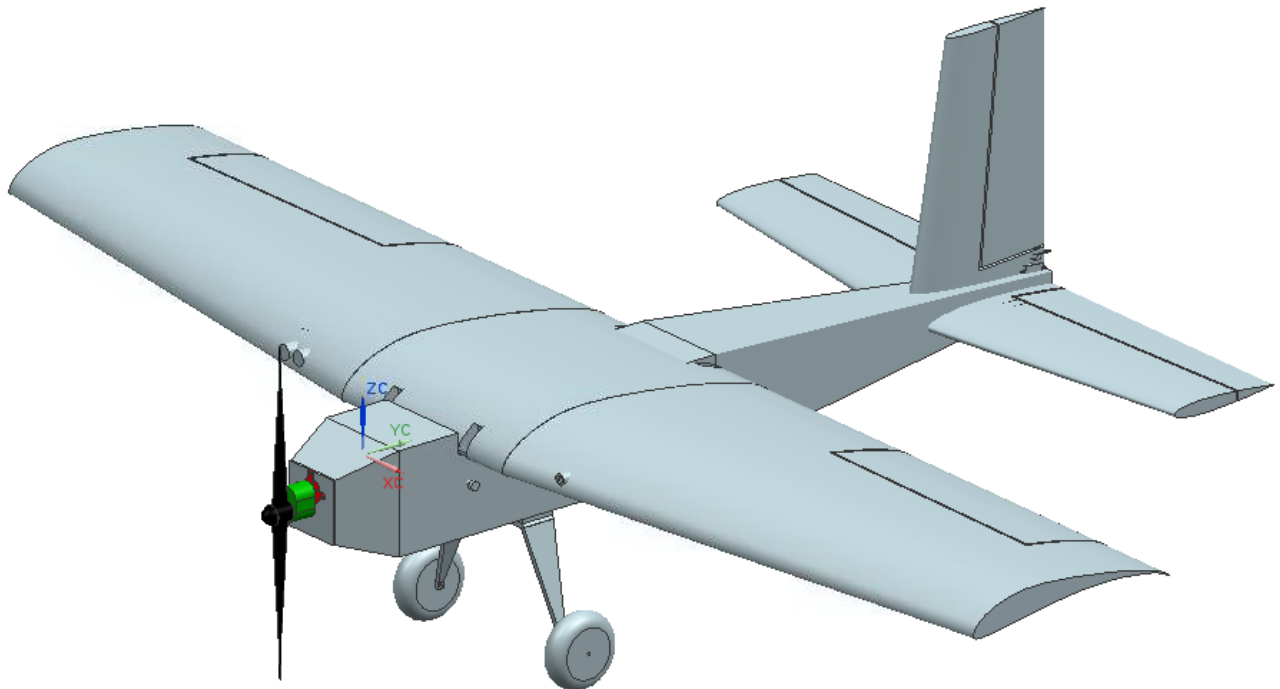


The Momma Goose

Final Design Report

AAE 45100 Senior Aircraft Design
Dr. DeLaurentis
Fall 2015
Purdue University



Team Member Names and Signatures

Atayurt, Emily - Team Leader/Dynamics and Controls

Date

Egley, Bryce - Dynamics and Controls

Date

Lemcherfi, Aaron - Aerodynamics

Date

Paepflow, Andrew - Propulsion

Date

Sarmiento, William - Structures

Date

Siefert, Andrew – Design

Date

Table of Contents

Executive Summary.....	4
1 Introduction.....	5
2 Aerodynamics.....	5
2.1 Introduction.....	5
2.2 Initial Design & Analysis.....	5
2.2.1 Initial Sizing.....	5
2.2.2 2D Design and Analysis.....	6
2.3 3D Design and Analysis.....	7
2.4 Selected Design & Conclusions.....	9
3 Propulsion System.....	10
3.1 Introduction.....	10
3.2 Design Process.....	10
3.3 Motor and Speed Controller Selection.....	10
3.4 Propeller Selection.....	12
3.5 System Testing.....	12
4 Weights and Structures.....	12
4.1 Introduction.....	12
4.2 Physical Properties.....	13
4.3 Wing.....	13
4.4 Fuselage.....	16
4.5 Tail Section.....	17
4.6 Landing Gear.....	17
5 Dynamics and Stability.....	18
5.1 Introduction.....	18
5.2 Static Stability.....	18
5.3 Dynamic Stability.....	20
5.4 Flight Characteristics.....	20
6 Sense and Avoid.....	21
6.1 Introduction.....	21
6.2 Conceptual Approach.....	21
6.3 Systems Layout and Flow.....	21
6.4 Pilot Acknowledgments.....	22
7 Economics.....	22
7.1 Cost Breakdown.....	22
7.2 Schedule and Man Hours.....	22
8 Conclusion.....	23
9 References.....	24
 Appendix A – Aerodynamics.....	 25
Appendix B – Propulsion System.....	28
Appendix C – Weights and Structures.....	33
Appendix D – Dynamics and Stability.....	43
Appendix E – Sense and Avoid.....	56
Appendix F – Economics.....	57

Executive Summary

The Momma Goose is a lightweight, fixed wing, ultra-efficient, electric powered, Unmanned Aerial System. It is designed to be stored in a 24" by 18" by 17" container, then assembled on the airfield within 10 minutes. The Momma Goose will take off in less than fifty feet at a climb angle greater than 25 degrees with a two pound payload. It will climb to an altitude of 300 feet and prove its stall speed capabilities of less than twenty three feet per second. The Momma Goose will then descend to 80 feet where it will complete the sense and avoid mission. This mission consists of sensing a balloon in its flight path then signaling the pilot. The pilot will activate an autonomous maneuver when signaled and the Momma Goose will autonomously avoid the balloon by 50 feet. After completion of the sense and avoid mission, the Momma Goose will return to 300 feet and to complete the endurance of 12 minutes then descend to a land.

The wing was designed with a large tapered wing span to create enough lift at the low speeds to carry the payload while reducing the drag due to lift. The airfoil chosen was the S1223 which was designed to create high lift at low speeds and angle of attack. The wing will be in three section in order for it to fit into the box. The middle of the wing will be square to make the placement of it on top of the fuselage easy while the other two sections will taper down.

The propulsion system uses the combination of a small motor to create a large RPM, a gearbox, and a large diameter propeller. This configuration is used in order to reduce weight and increase the efficiencies of the motor and propeller. The propeller has a 14 inch diameter and 12 inch pitch to create the maximum thrust possible.

The fuselage is made of thin foam and tapers down to a smaller size to save weight. It will be two pieces in order for it to fit into the container. These pieces will be connected together using carbon fiber rods going through each piece with rubber bands connecting them together. The nose of the fuselage will be a pyramid with the pointy end removed in order to attach the propulsion system to it. The wing will be fiber glassed in order to handle the loads created in flight. The sections of the wing and the tail will be connected using carbon fiber rods and magnets. The wing will be connected to the fuselage with rubber bands and rubber band rods similarly to how the two pieces of the fuselage come together. The tail will be connected by putting carbon fiber rods through the horizontal stabilizer, vertical stabilizer, and end of the fuselage. The landing gear is in the tail dragger configuration with carbon fiber spars to save weight.

The tail being used is a conventional design. There will be four control surfaces on the Momma Goose, an elevator, a rudder, and two ailerons. Four servos will be used to control all of these surfaces.

Due to the high lift created by the specific airfoil chosen, flaps will not be used to aid in takeoff.

There are two sense and avoid equipment being used. The first is a LIDAR which is a laser based measuring device. The second will be a camera in combination with a Raspberry Pi computer which will calculate the distance of an object based on the size of the pixels from the camera. The camera and the LIDAR will be placed on the wing in opposite locations to counteract each other's weight. They will be placed in the wing similar to headlights in a commercial aircraft.

Takeoff Weight	6 pounds
Wing Geometry	
Wing Span	60 inches
Root Chord : Tip Chord	13.5 inches: 10 inches
taper ratio	0.74
Tail Geometry	
Horizontal Stabilizer span	28.5 inches
Horizontal Root Chord : Tip Chord	7 inches : 5 inches
Vertical Stabilizer Span	11.5 inches
Vertical Root Chord : Tip Chord	7 inches : 5 inches
Fuselage	
Length	37 inches
Cross Section	4.5 inches by 4.5 inches
Tapered Cross Section	1 inch by 1 inch

Table 1.1: Key design parameters on the Momma Goose.

1 Introduction

Small UAS's are of popular interests for civil and commercial sectors. In the civil area they can be used for security footage in public safety as well as border patrol. In the commercial industry they are already used by hobbyists but can also be used for simple tasks like crop dusting. Problems with obstacle avoidance can arise when using these systems. Based on this problem, our challenge was to design a lightweight UAS with the capability to sense and avoid an object in flight.

This report consists of the summary of the design phase of this design challenge. The report is broken up into six subjects: aerodynamics, propulsion, structures, controls and stability, sense and avoid, and economics. Each will explain in detail how the Momma Goose will complete its objective.

2. Aerodynamics

2.1 Introduction

This chapter presents the process our team worked through to develop our UAS's aerodynamic system. Within this chapter we will present highlights from our Initial Sizing, 2D Design & Analysis, 3D Design & Analysis, and our Final Design Selection stages. Additionally, this chapter will serve to point out

how various aspects of our aerodynamic system will positively or negatively impact, or be impacted by, other systems within our UAS.

As readers of this chapter begin to digest its content, we would advise that he or she remains cognizant of the Team 3 Aerodynamic Design Process given in Appendix A of this report, which gives a high level view of our aerodynamic system design process.

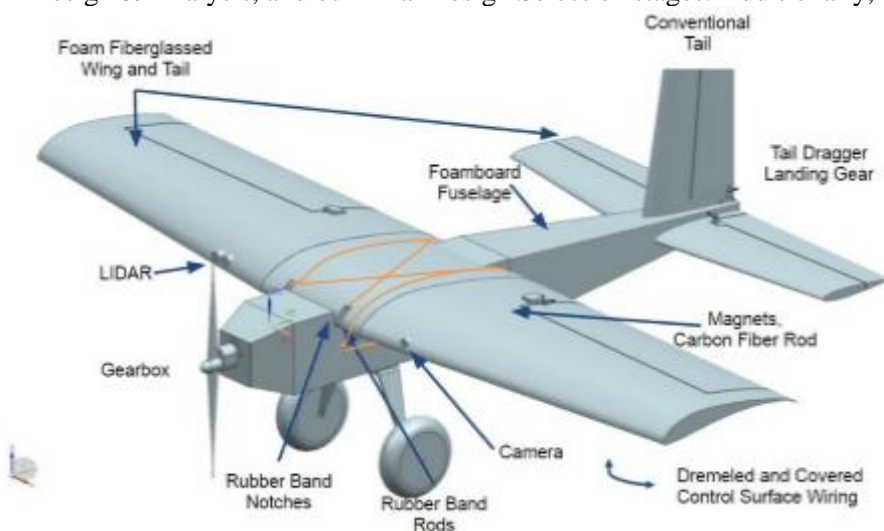


Figure 1.1: Key design parameters on the Momma Goose.

2.2 Initial Design & Analysis

2.2.1 Initial Sizing

To size our aircraft, we started by reviewing our RFP and making an educated guess of the type of aerodynamic and propulsion systems that we would need. This then allowed us to design a paper design of our UAS and thus obtain a first pass weight estimate. By obtaining a first pass weight estimate, we were then more capable of determining specifications of our aerodynamic system such as the wing's planform area, lift coefficient, as well as the velocity it would have to operate at in order to complete the mission at hand. Once a rough idea was determined for how much lift we would be required to generate, we then acknowledged that we had no incentive to design a UAS that is, speedy or highly maneuverable (beyond the requirements called out in our RFP). As such, we decided to develop a wing design that would have the largest possible wing planform area that could still feasibly be built, produce adequate structural integrity, fit in our shipping container, and produce optimal aerodynamic qualities (e.g. high L/D, low drag at cruise conditions, etc.). After a brainstorming session and measuring the dimensions of our allotted shipping container, we determined that the maximum wingspan we would confidently be able to produce for our wing would be roughly 60 inches. This number was developed by determining that we could feasibly develop a wing with three 20" sections.

Before we started our 2D analysis we had to first determine a Reynolds Number range at which we would perform our analysis. To determine this however, we needed to first determine our chord length and cruise velocity. This was done via making a first pass estimate at our chord length. We then used this chord length in conjunction with our estimated max wingspan length and the lift equation (see Appendix A) to determine our UAS's cruise velocity. With a first pass chord length of 14" and a cruise velocity ranging somewhere between 20 ft/s and 40 ft/s, we found our Reynolds number range to be around 150,000 – 300,000.

2.2.2 2D Design and Analysis

Due to RFP requirements, we determined that our wing's design should incorporate an airfoil which is capable of producing a high Cl/Cd value at cruise conditions. Doing so will enable our UAS to travel at a lower velocity which will in turn lower the propulsion system's weight needed to power our UAS and thus further lower the lift required of our aerodynamic system (i.e. if we need less power from the from the propulsion system, we can reduce the weight of its motor and battery).

Via a quick literature review, we have determined that in order to overcome the rather poor performance characteristics of traditional airfoils at the low Reynolds Number range our aircraft will be operating at we should analyze the benefits of airfoils with a high camber and thin profile¹. As a result we looked at the airfoils given in Figure 2.1, below. In addition we also looked at a commonly used, standard low Reynolds number airfoil, a NACA 2412, as our baseline.

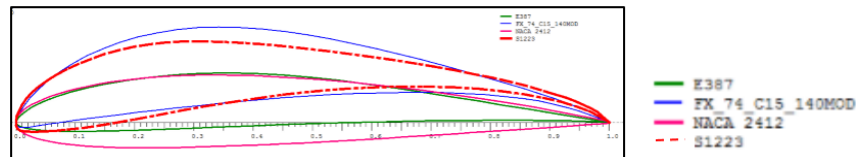


Figure 2.1: Profile of Airfoils Selected for Further Design Analysis

Among the airfoils we compared, the NACA 2412 had the least amount of camber and was the thickest. As a result we expected it to have a relatively low lift coefficient at a low angles of attack as compared to the other airfoils. We also expected the higher camber airfoils to have a slightly lower stall angle of attack since they were already producing a large pressure differential between the top and bottom surfaces of the airfoil at a zero angle of attack and only a finite pressure differential can be generated before aerodynamic stall occurs. Due to the requirements called out in our RFP, we deemed it more desirable for our selected airfoil design to have a high coefficient of lift during steady level flight, while we will be slightly less concerned with stall angle of attack capabilities (beyond those that enable us to meet takeoff flight path angle requirements). As given in Figure 2.1, the FX 74 C15_140 MOD airfoil was the thinnest and highest cambered airfoil, therefore we expected it to have the best aerodynamic performance characteristics at low angles of attack. Additionally the geometry of this airfoil promoted the lightest wing design. This airfoil however posed various problems associated with its structural integrity capabilities and ease of manufacturing traits. Conversely, the E387 airfoil was thickest high camber airfoil we analyzed and served as our “lower bound” high camber airfoil. Benefits of using this type of airfoil include structural integrity benefits and ability to mount control structures. At this stage in our design process we were primarily concerned with L/D and coefficient of lift values. As such, we ran an analysis of the selected airfoils at conditions representative of cruise conditions. Results of these values are presented in Table 2.1.

Table 2.1: 2D Analysis Results

Airfoil	$C_l @ \alpha=0$	$C_{l,max}$	$\frac{L}{D} @ \alpha=0$	$\frac{L}{D_{max}}$
NACA 2412	.275	1.35(@ $\alpha=13$)	30	75(@ $\alpha=6$ deg)
S1223	1.12	2.1 (@ $\alpha=14$)	65	70(@ $\alpha=5$ deg)
FX_74_C15_140_MOD	1.15	2.1 (@ $\alpha=12$)	55	90(@ $\alpha=5$ deg)
E387	.4	1.2 (@ $\alpha=11$)	40	40(@ $\alpha=11$ deg)

In summary we found that the lower chamber, thicker airfoils gave lower zero angle of attack lift coefficients but were more capable of producing lift over a larger range of angle of attack. We found that higher camber, thin airfoils were optimal in their ability to produce both high lift coefficients at zero degrees angle of attack, overall max C_L values, and both zero angle of attack L/D and max L/D values. After using the hot wire foam cutter in ARMS 2098 to create a FX_74_C15_140_MOD wing, we immediately determined that this airfoil would have significant structural integrity concerns due to how thin its trailing edge is. From further review of our 2D analysis results and from actually producing a S1223 airfoil wing we determined that it would be our airfoil of choice moving forward with a 3D analysis.

In order to increase simplicity for our final design, we have determined to employ a NACA 0012 for our horizontal and vertical stabilizer. The thicker NACA0012 airfoil will allow for ample structural integrity and mounting space of control surface hardware.

2.3 3D Design and Analysis

As it currently stands, our chosen aerodynamic system implements a wing with a span of 60", a chord of 13.5", and incorporates a S1223 airfoil. This served as our baseline wing planform as our team moved forward to determine an optimal taper ratio. For this analysis we looked at the effect of varying taper ratio from 0.5 to 0.9. Additionally we also analyzed the how sweeping the entire wing planform verses only sweeping the outer wing section altered our wing's overall aerodynamic performance. Results of this analysis are given in Figure 2.2. This figure refers to wing planforms that are swept along the entire wingspan as "Full Wing Taper" and refers to wing planforms that are only swept along their outer two wing sections as "Half Wing Taper". For clarity, only key taper ratio values are plotted in Figure 2.2. Also for clarity, the "Half Wing Taper" ratio results are only given in the figure below for the final selected taper ratio.

We noted from Figure 2.2, that C_L/C_D values tended to peak and C_D values tend to be near their minimum values near an angle of attack of zero. These were deemed as preferred aerodynamic system characteristics and reaffirmed our team's airfoil selection decision. Further we note that we decreased the taper of our design, aerodynamic performance increased. However, after manufacturing wings with lower taper ratios we have determined that we structurally have a lower bound on how much taper we can incorporate. In addition due to the size constraint of our wing imposed by shipping requirements we were also limited by how long our wingspan would be. Therefore we needed to ensure that overall planform of our wing provided enough surface area to produce enough lift to keep the UAS aloft. This also posed a lower bound on how far we could decrease our wing's taper ratio.

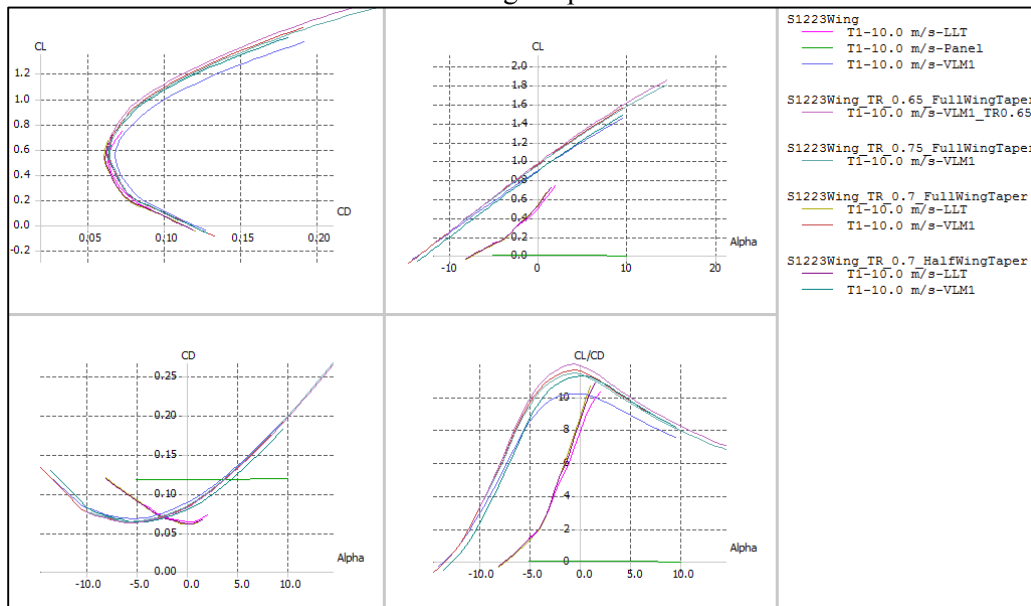


Figure 2.2: Effect of Taper Ratio

After performing this study and considering other design constraints, we determined that the incorporation of a taper ratio of approximately 0.7 was optimal. Due to the need to maintain structural integrity near the fuselage, provide adequate mounting space for sense and avoid equipment, maintain an appropriate wing planform surface area, and to take advantage of aerodynamic benefits of incorporating wing taper, our team opted to incorporate the “Half Wing Taper” design. As given in Figure 2.1, this design gives us performance characteristics somewhere in the middle of having a fully tapered wing and having a zero degree swept wing. From producing this wing at full scale in ARMS2098 we have also determined from physical testing that this design will be capable of handling the loading conditions expected to be applied to it during operation. After further analysis and iteration cycles are team determines that we could further increase the

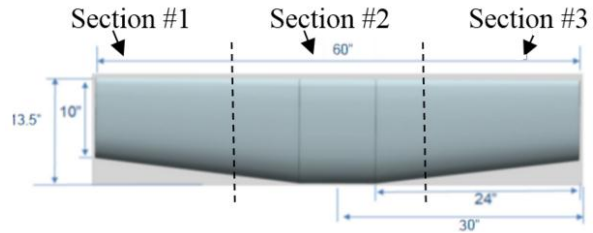


Figure 2.3 Final Wing Planform

Table 2.2: Aerodynamic Parameters

Aerodynamic Parameter	Value
Taper Ratio	0.74
Aspect Ratio	5.10
Dihedral Angle	0
Planform Area	4.9 ft ²
Wetted (Aircraft) Surface Area	17.6 ft ²

wingspan over which taper is present. Keeping with the initially selected 0.7 taper ratio design selection, our team’s final wing incorporates taper over the outer 24” of the wingspan. Our final selected wing design is given below in Figure 2.3.

While manufacturing the wing planform given above, with the hot wire foam cutter in ARMS 2098, our team noted that there would be a significant level of difficulty associated with adding dihedral to our design. Further, our team concluded that adding dihedral would lower the structural integrity of our system as a whole and only provide marginal increases in stability. As a result, our final design does not incorporate dihedral. Aerodynamic parameters

representative our final design are given in Table 2.2.

XFLR5 and STAR-CCM+ were used to determine additional 3D aerodynamic parameters. These methods were then validated via comparing them to results obtained from acquiring experimental L/D data. Experimental data was collected building and flying a glider prototype. First pass results of this comparison are given in Table 2.3

From table 2.3, we noted that however XFLR5 LLT and Star CCM+ results appear to more closely match experimental results, there is still a considerable amount of error associated with these methods. We should note here that there is a long list of potential sources of error in using these solution techniques. First and foremost, we should note that however our experimental data was collected during transient (i.e. decelerating) flight conditions, our analytical results assumed steady level flight. Further error could have been produced due to the fact that XFLR5 does not account for viscosity effects. In addition, a large

Table 2.3 3D Analytical & Experimental Results

L/D Analytical vs. Experimental Comparison		
	L/D	Percent Error (experimental as baseline)
Star CCM+	9.25	37%
XFLR5 (VLM)	11	63%
XFLR5 (LLT)	7.9	17%
Experimental	6.75	na

Aerodynamic Parameter	Value
$C_{L,max}$	2.0
$C_{L,\alpha=0}$	0.42
$C_{L,\alpha}$	0.16 (1/deg)
C_{D0}	0.06
$C_{D,\alpha=0}$	0.123
$\frac{L}{D}_{\alpha=0}$	6.8
$\frac{L}{D}_{\alpha=max}$	4.8

Table 2.4: Aerodynamic Values of Final Design

part of the error associated with first pass STAR-CCM+ results was believed to be a result of inadequate mesh refinement. However, since STAR-CCM+ is more capable of modeling the flow physics that are to be expected during physical flight, it was pursued as our main analytical tool. After a mesh refinement study was conducted, which enabled STAR-CCM+ results to be within 10% (deemed to be acceptable since we were modeling the steady state case) of the initially collected experimental data we utilized it to obtain the aerodynamic values given in Table 2.4.

Note*: These are CFD generated values for the full aircraft (i.e. wing, fuselage, tail). External features (wiring, the propeller, servos, etc.) were not modeled to give above results. These results are also given in the CL vs. Alpha and drag polar plots given in Figures 2.4 and 2.5.

From these aerodynamic parameters, we have determined that our final design will be able to successfully operate in the region labeled with red square in the constraint design given in Figure 2.6. Since this operating region is located within the allowable design space, our final design will be able to meet the requirements put forth by our RFP. The code that was used to develop our constraint diagram is given within Appendix A.

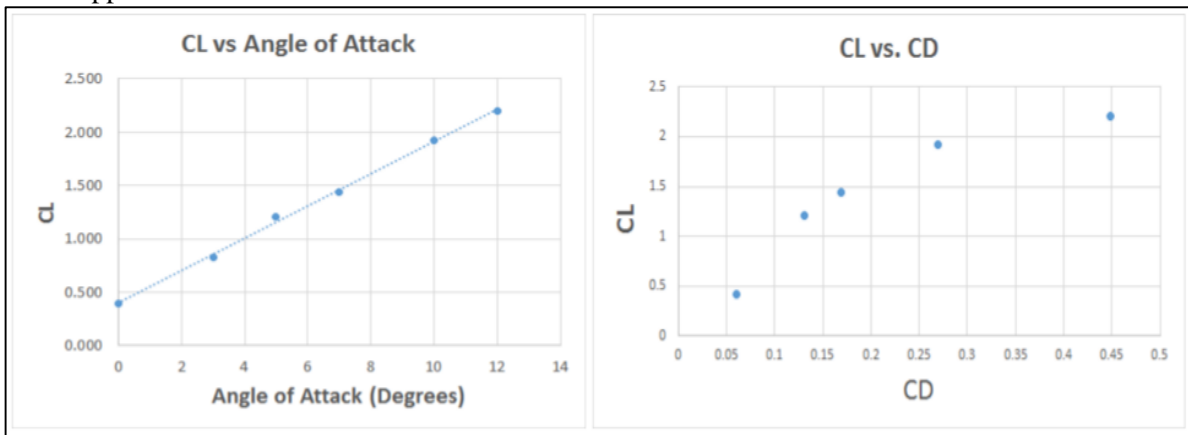


Figure 2.4-2.5: Final Design CL vs. Alpha (Left) & Drag Polar Plot (Right)

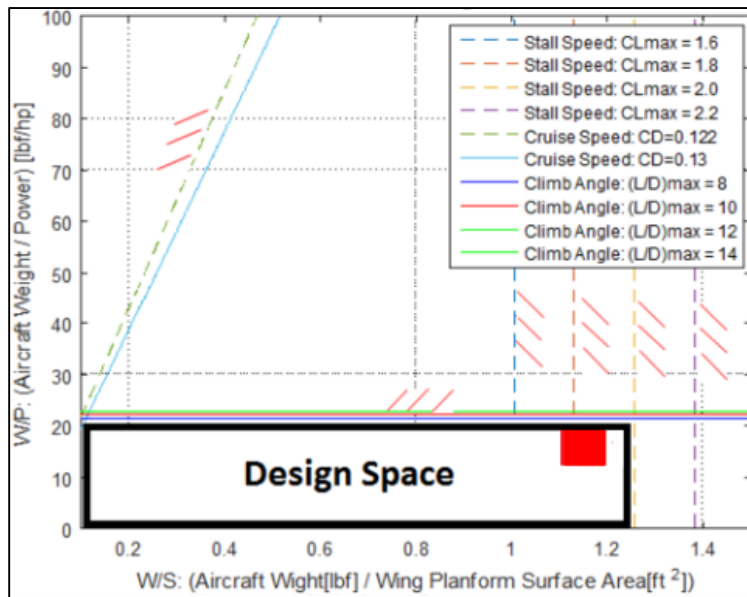


Figure 2.6: Final Design Constraint Diagram

2.4 Selected Design & Conclusion

Due to its high level of aerodynamic performance characteristics at cruise and near cruise conditions, our team has determined to incorporate a S1223 airfoil into our final wing design. Our wing incorporates three separate wing sections which will allow it to meet the shipping constraints presented in Our RFP. These wing sections are defined in Figure. 2.3 As given in Figure 2.2, this design gives us performance characteristics somewhere in the middle of having a fully tapered and zero degree swept wing. From producing this wing at full scale in we have also determined from physical testing that this design will be capable of handling the loading conditions expected to be applied to it during operation. Through analytical methods validated by experimental results we have

been able to produce the results given in Table 2.4 and Figures 2.4-2.5. From analyzing these results, our team confidently believes that our final UAS design promotes aerodynamic qualities which will allow us to meet all aspects of our mission, as outlined in our RFP.

From these aerodynamic parameters, we have determine that our final design will be able to successfully operate in the region labeled with red square in the constraint design given in Figure 2.6. Since this operating region is located within the allowable design space, our final design will be able to meet the

requirements put forth by our RFP. The code that was used to develop our constraint diagram is given within Appendix A.

These results are also given in the CL vs. Alpha and drag polar plots given in Figures 2.4 and 2.5.

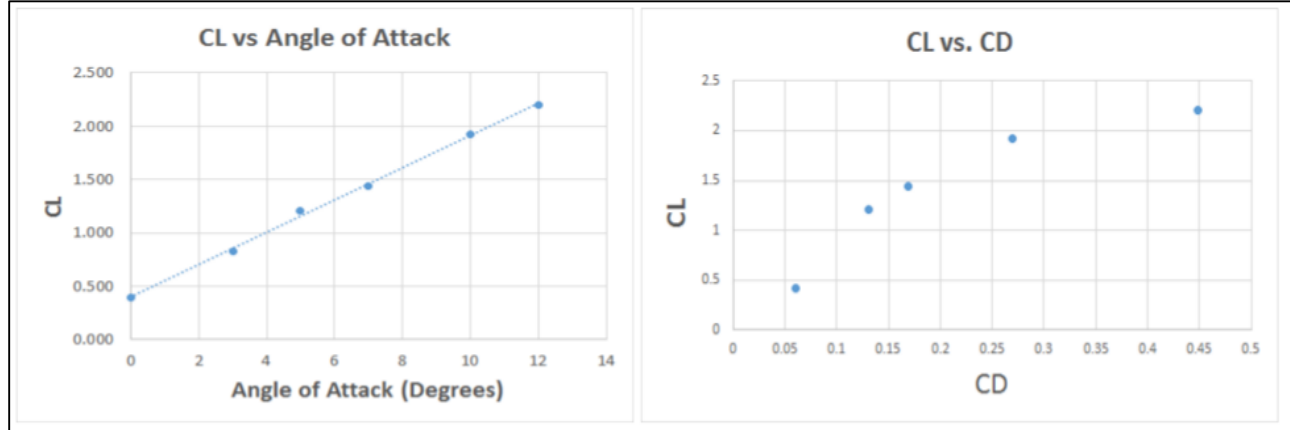


Figure 2.4-2.5: Final Design CL vs. Alpha (Left) & Drag Polar Plot (Right)

3. Propulsion

3.1 Introduction

The objective of this mission that is most pertinent to propulsion is the requirement to fly for 12 minutes. Additional power requirements include minimum stall velocity and maximum takeoff distance. Both of the last two requirements are met in the constraint diagram. We used the constraint diagram to ensure that our power plant system was sufficient in order to meet the requirements of the mission while at the same time, minimizing the power plant so that our overall weight and size could be reduced.

3.2 Design Process

Using a vehicle weight of 6.5 lbs., incorporating a safety factor, a wing length of 60 in, and a chord of 13.5 in, basic vehicle parameters were calculated. Additional wing data such as Oswald's Efficiency factor and zero lift drag were needed. In order to find the most efficient flight conditions, in our case least power consumption, we found a velocity in order to maintain level cruise which consumed the least amount of power. Additional vehicle weights were considered and run in order to notice a trend in vehicle power needs with a range of vehicle weights.

Dr. Andrisani's code³, Main_System_Design, was used in order to find maximized efficiency design points. This code must be modified before use. Propeller data from APC must be changed to reflect the propeller class being used. The first code function finds the aerodynamic conditions of lift and drag and finds the velocity required to fly the system with payload while using the least required power input. Our vehicle was shown to fly with the least effort at 27 ft/s.

3.3 Propeller Selection

The second portion of the code pertained to the propeller selection. Aside from inputting vehicle parameters stipulated previously, propeller type must be considered. The diameter, blade count, and pitch angle all play significant roles. The code initially contains a data sample for an APC propeller with a specified pitch to diameter ratio, Tau, of 0.857. A table of thrust coefficients and their corresponding advance ratios are plotted. This table of values needs to be updated to the family of propellers chosen for the design.

Several propeller families were chosen in ranges from 10"x 7" up to 14"x 12". The 14" propeller was the upper limit due to ground clearance and vehicle size. The remaining portions of the code were not needed at this point for this application.

Figure 3.4.1 shows the APC Thin Electric 14"x12" two blade propeller chosen. Due to our low velocity, a small propeller showed lower than expected efficiencies. For reference, a 10"x7" propeller showed only a .53 efficiency at 27 ft/s. This was not acceptable. While we realized that minimized power consumption was the main goal for this analysis over propeller efficiency, this efficiency was so low, that a motor had to compensate for the power losses in the propeller. It was noticed that a higher vehicle velocity and/or larger propeller diameter would increase advance ratio, J , and lead to higher efficiencies. By the equation $J=V/(nD)$ where V is cruise velocity, n is propeller rpm, and D is propeller diameter. A larger diameter D alone would decrease J , but the n component of RPMs creates a larger effect. The RPM of a larger propeller is much smaller than that of a smaller propeller.

In summation, a slower turning larger propeller for low velocity flight results in the highest efficiency. Figure 3.4.2 shows the trend that J has on efficiency and thrust and power coefficients, C_T and C_P , respectively.

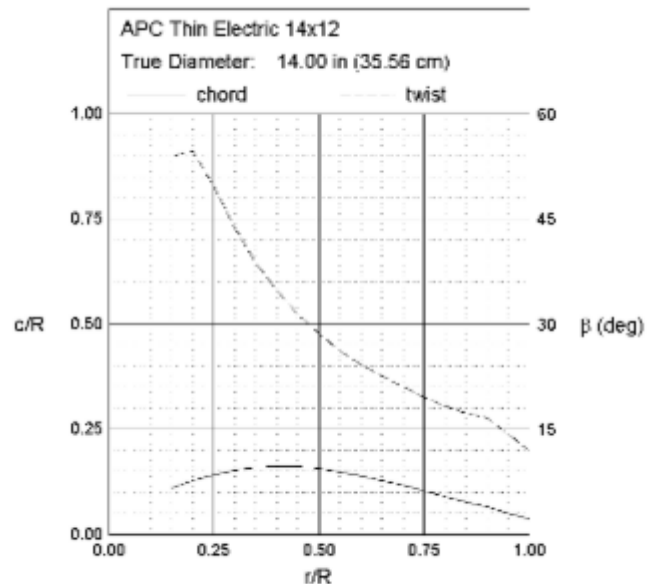


Figure 3.4.1 Propeller Pitch Curve

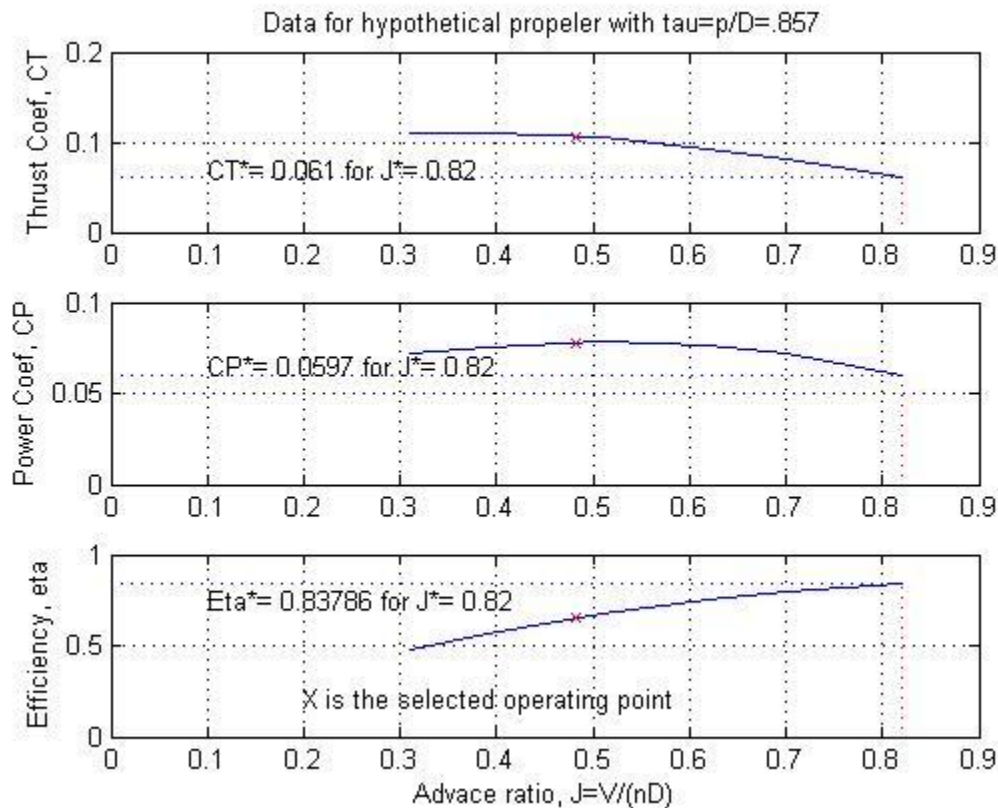


Figure 3.4.2: Advance Ratio

The advance ratio J curve shows a range of velocities. The star in the curve shows the point chosen for our velocity of 27 ft/s. At this velocity, our propeller has an efficiency of .65. At its maximum, the propeller would achieve an efficiency of .82 although the velocity of 45m/s that corresponds with this efficiency requires double the power input. (Note: the “X” denotes the design) The chosen velocity requires only 0.08 HP. Note that this power requirement shows only for cruise condition. Takeoff and climb will require about 1.0 lbf of thrust. Based on the APC experimental data, the power needed for this would be 0.1 HP². For this, a variable power motor with a peak of 0.35 HP was chosen. The motor power is variable with input voltage so that it can be operated in an efficient power band while also having more power than needed. Though .35 HP is above needs, total system efficiency will lower this value and motors any smaller would have severe efficiency losses as well as lower build quality.

3.4 Component Selection

The motor chosen was an out runner style. An out runner is a brushless motor where the motor casing turns and the center shaft is held fixed. This allows for a higher torque from a smaller motor. This motor is our best option for power requirements due to its small size and battery needs, but it spins at too high of an rpm. Our propeller needs to spin at 3000 rpm while the motor at 14.8 volts will spin at 16,200 rpm. A simple reduction gearbox will reduce the shaft speed and multiply the torque. We chose a gear ratio of 3.8 as this was the closest commercially available product to our needs. This also allows us to fly cruise at 70% power for the correct RPM and have plenty of reserve power for maneuvers.

The last aspect to the initial propulsion calculations pertain to battery sizing. The main power requirement is duration. Our tightest design criteria is weight. A Lithium Polymer battery was chosen due to its superior voltage retention and better thermal properties of NiCd or NiMH. A 4 cell, 14.8 v, 3700 mAh battery was chosen. At the maximum power output rating of the motor, this battery allows a 14 min flight time which goes above the mission specification and leaves a window for lower battery performance due to colder temperatures.

3.5 System Testing

The selected system needs to be proven before flight. The combination of an out runner and gearbox is not a common option. Smaller electric motors spin fast but have low torque outputs. The gearbox is a mechanical means of converting the high rpm into a useable lower rpm with a higher applied shaft torque. The out runner motor is designed to eliminate the need for a gearbox and offer higher efficiencies. Unfortunately, due to the factors associated with minimizing weight and maximizing efficiencies, the ideal motor size was not up to the task of turning the propeller on its own. The propeller is RPM limited to about 4500 RPM and for the motor to spin at that speed directly, there is not enough power or torque to compensate. Thus, there is a need for a gearbox.

The plan of action is to build and test the system on the ground to ensure fitment. The gearbox is being slightly modified. The motor selected has an output shaft of diameter 3mm. This size is small for most out runners, but this allows the gears to fit onto the motor shaft. This power combination was theoretically designed and experimentation pre-flight will confirm the setup. The alternative would be an inefficient approach of using an industry standard larger motor. We decided against the industry standard as we knew we could develop superior combination with the added benefit of lower weight and lower power consumption with the tradeoff of slightly higher complexity.

4 Weights and Structures

4.1 Introduction

In determining the structural design for the Momma Goose, several key mission requirements were taken into account. These key requirements deal with four categories, including ease of deployment, overall weight, cost, and manufacturing. One of the key mission requirements required the aircraft design to be as light as practical, while carrying a 2lb payload. This drove the need for the use of lightweight, yet strong materials for the fuselage and wing structure of the aircraft. The total weight of our aircraft, including the payload and internal components is approximately 6 lbs. (see Appendix C). The aircraft wing structure was

made up of styrene foam, lightweight carbon fiber rods that acted as wing spars and fiberglass coating. Fiberglass was used as reinforcement for the outer surface of the wing where it would be needed in critical areas, such as the thin trailing edge. Styrene foam was used to get a precise airfoil geometry for the wing, as well as to create the horizontal and vertical tail stabilizers. The ability to be stored and transported in a plastic storage container with dimensions $24\frac{1}{4} \times 18\frac{5}{8} \times 17\frac{5}{8}$ was a key requirement that led to the use of both a detachable fuselage, wings landing gear and payload. To land the Momma Goose safely on the ground, the aircraft made use of sturdy and lightweight landing gear struts. Comprehensively, the budget of the project limited the structural material to be inexpensive and easy to manufacture. This led to the dimensional simplicity of our aircraft, which was beneficial in the Momma Goose's manufacturing and maintenance.

4.2 Physical Properties

In order to perform structural analysis for the Momma Goose, key physical properties of the materials used were collected. Table 4.2.1 lists the principal materials that make up the key structural components on our aircraft.

The properties for the polystyrene foam was obtained online through Northwest Foam Products¹⁰, whose foam products similarly matched to the foam used for our aircraft. The woven fiberglass for the coating on our wing was bought through an online source named ACP Composites¹¹, while its properties, as well as those for the carbon fiber, were obtained through an external source named Performance Composites¹². These material properties demonstrate the approximate values for the material used on our aircraft and provide an accurate way of determining how much loads our structure can withstand, both inflight and on the ground.

Table 4.2.1 Material Properties

Material	Young's Modulus [lb/ft ²]	Tensile Strength [lb/ft ²]	Compressive Strength [lb/ft ²]	Density [lb/ft ³]
Polystyrene Foam	46080	7350	3456	1.55
Plain Weave Polyester - 45% E-glass	2.30e8	1.51e7	9.94e6	97
Carbon Fiber	1.56e9	4.32e7	1.20e7	97
Nylon Plastic	1.44e6	-	-	-

4.3 Wing

The wing on the Momma Goose is responsible for carrying all loads during flight while maintaining its structural integrity and cambered shape. Figure 4.3.1 shows a top view layout of the wing structure for our aircraft. One of the key things to note is that the wing is divided into three separate 20" sections in order to meet the storage container dimensional requirement. The wing itself is constructed out of the polystyrene foam board, which is then fiberglass coated for reinforced strength.

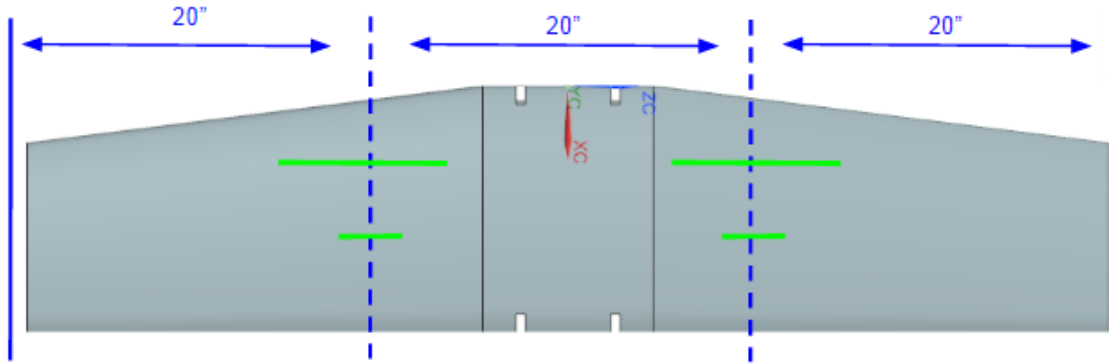


Figure 4.3.1 Top View Layout of Wing Structure

Since the wing is divided into separate sections, carbon fiber spars are used to connect the three sections. Four hollow carbon fiber spars of circular cross section (shown in green) are placed along channels on the bottom of the wing. These channels are manufactured prior to the fiber glassing of the wing with a dermal and hot soldering iron to melt away remaining foam. The hollow carbon spar will be laid into the foam and encased in an epoxy/micro-balloon mixture to hold the spar firm, thus making the hybrid into one structure as well as to re-mold the cut face back into a smooth airfoil. The two carbon fiber spars closer to the leading edge each have a length of 10", while the shorter spars behind these each have a length of 4". These spars have an inner diameter of 0.235" and will house a 0.218" diameter solid carbon fiber rod along the inside, which will provide the primary connection between the wing sections.

To keep the wing sections aligned and prevent any gaps at the areas of attachment, four round N48 neodymium magnets of 1/4" diameter and 1/16" thickness are attached to each of the inner portions of the wing sections. There will be 8 magnets per wing attachment, giving a total of 16 with a combined pulling force of approximately 5.5 lb. per wing attachment (see Appendix C). Figure 4.3.2 shows an internal side view of the wing with the magnets highlighted in pink, and the spars in green.

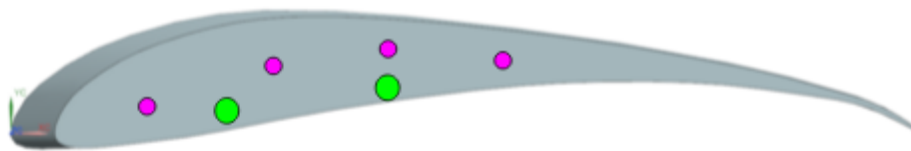


Figure 4.3.2 Internal Side View of Wing

As a conservative effort, the analysis of wing loads on the aircraft was performed using the properties of the fiberglass coating. The fiberglass was designed to support the bending loads applied at the maximum loading condition during flight, which occurs at the maximum lift from turning. The carbon fiber

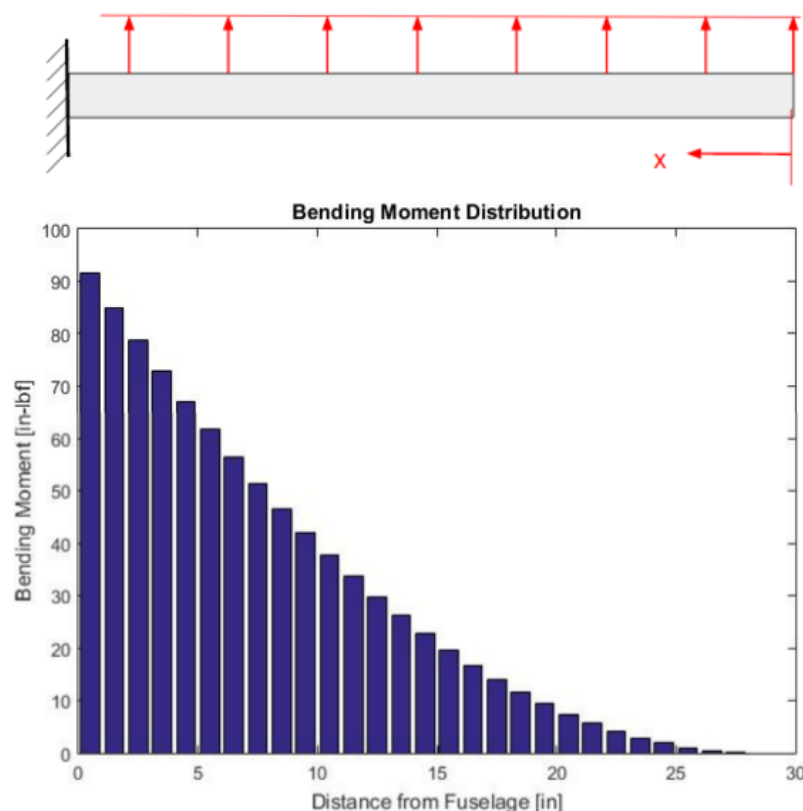


Figure 4.3.3 Beam Modeling and Bending Moment Distribution

spars, which exhibit both a tensile and compressive strength greater than that of fiberglass, are responsible for transferring the loads across the wing sections. Knowing the Momma Goose's estimated velocity while turning, along with the turning radius, weight of the aircraft and safety and loading factors of 1.5 each, the maximum lift from turning was calculated to be approximately 13.3 lbf (see Appendix C). Assuming an even lift distribution and modeling the wing as a cantilever beam, as shown in Figure 4.3.3, the maximum bending moment that would be experienced in flight at the wing root was calculated to be 91.47 in-lbf.

The minimum thickness of the fiberglass was obtained by using both the results of the bending moment analysis, as well as a wing twist analysis. To accomplish this, the airfoil was modeled as a hollow rectangular cross section, where the variable of interest was the thickness

of the walls of the hollow rectangle. The bending moment analysis uses the moment of inertia and bending stress equation to obtain the required thickness. The wing twist analysis used a combination of the torsion constant and max twist equation to obtain the required thickness for the fiberglass that would prevent the maximum wing tip twist angle from surpassing 1° . Both analyses were performed using a factor of safety of 1.5 (See Appendix C). While the bending moment analysis resulted in a required thickness of 0.0004 inches, the wing twist analysis demonstrated a need for a greater thickness of 0.0018 inches. The fiberglass chosen based on material availability and analysis results was a 1.4 oz., 0.0025" thick woven fiberglass, which provided a margin of 38.9% over the required thickness from the wing twist analysis.

4.4 Fuselage

The fuselage is composed of two separate cardboard foam sections that each measure 18.5" in length with a 4.5" square cross section. These cardboard foam sections are coated in a lightweight blue sheet for added structural rigidity and durability in case of an impact and are joined together with a combination of clear tape and hot glue. The dimensions of the internal components are what drove the height and width of the fuselage. Figure 4.4.1 shows where the two sections are joined together at the dotted red line. In order to attach these sections, a smaller square cross section (about 4.25" in length), is permanently attached only to the aft portion of the fuselage at the joining point, which serves as a connecting bridge between the two sections. To make sure the two sections remain together, two hollow carbon fiber rods (highlighted in orange) are placed on either side of the connecting sections. These rods are wrapped around with a tight rubber band, which will act as the final force to push the two sections together.

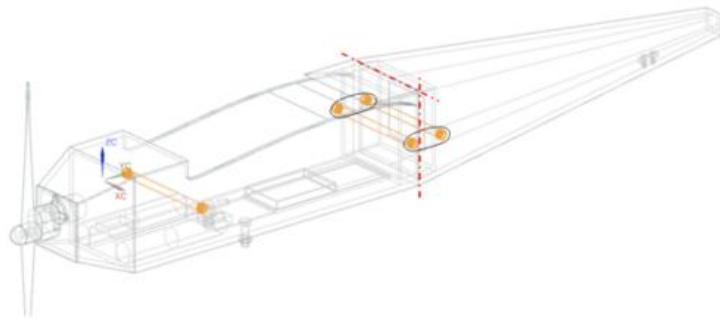


Figure 4.4.1 Fuselage Sections

For the firewall attachment, a thin piece of wood that is attached flush to the flat nose of the aircraft with a set of nylon nuts and bolts. This piece of wood represents the front piece of a lightweight wooden 'box' that will take the form of the forward nose of the fuselage (on the inside) and provide support for the motor and engine mount. The edges of the excess front tapered fuselage (our manufacturing method will

allow for this) are slit and bent inward toward the fuselage to act as a base where the thin piece of wood is attached. The bended edges will be reinforced with epoxy and resin adhesive to ensure the fuselages structural integrity.

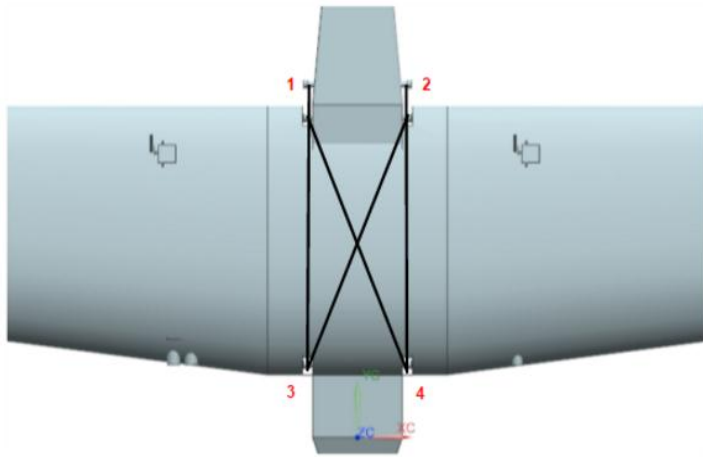


Figure 4.4.2 Rubber Band Attachment Configuration (Top-View)

has four notches (labeled in the figure) that securely hold the rubber bands in place (two bands per notch). Additionally, one rubber band is placed in the longitudinal direction of the fuselage along each side of the wing and held in place by two carbon fiber rods (one of which is the same rod that holds together the fuselage sections).

To securely attach the wing centerpiece to the fuselage, the top of the fuselage has a cutout in the geometry of the bottom portion of the wing's airfoil. There cutout, aside from acting as the 'bed' for the wing center section, also acts as an opening on the top so that the internal components can be easily accessed. Once the wing is placed on top of the fuselage, four rubber bands are used in an x-configuration, as seen in Figure 4.4.2. The wing centerpiece

4.5 Tail Section

The horizontal and vertical tails are constructed with a NACA 0012 airfoil shape and made out of the same styrene foam. The horizontal stabilizer is manufactured into two parts that will be joined together at either sides of the fuselage. For structural support, the horizontal tail consists of two carbon fiber spars

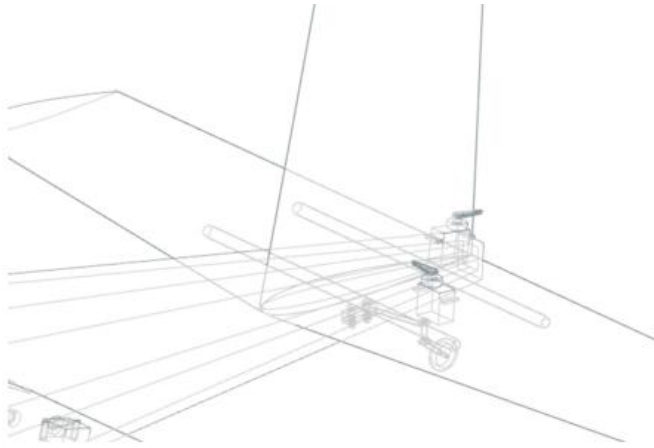


Figure 4.5.1 Horizontal & Vertical Tail Attachment

running parallel to each other that traverse the fuselage cross section at the aft of the plane (about 1.8" in width) and continue on into the sides of the horizontal stabilizer sections. The spars, of identical cross sectional dimensions as the wing spars, were chosen for their lightweight characteristics and to handle any critical stresses along horizontal tail that may be seen from any unforeseen hits, bumps, or hard landings. For added stiffness, a small portion of the ends of the rods are wrapped with a thin layer of tape to prevent the stabilizers from sliding in place. Figure 4.5.1 shows this connection.

The vertical stabilizer has two arches cut into the bottom of it (the section that is hidden away inside the fuselage) to have it fit around the carbon fiber spars used on the horizontal stabilizer. For part of the vertical stabilizer to be placed inside the fuselage, a proportional opening will be cut into the top of the aft section of the fuselage. Two pairs small wooden blocks, along with two nylon bolts and screws, located inside of the fuselage will act almost as a 'clamp' to hold down the vertical stabilizer at its trailing edge and leading edge.

The vertical stabilizer has two arches cut into the bottom of it (the section that is hidden away inside the fuselage) to have it fit around the carbon fiber spars used on the horizontal

4.6 Landing Gear

The Momma Goose features fixed landing gear with a tail dragger configuration. With the center of gravity located at 9.35" from the nose of the aircraft, we needed to make sure the front landing gear was placed in an optimal location to prevent forward tip over. The main landing gear, made of carbon fiber (Figure 4.6.1), is located approximately 6.5 inches from the nose of the aircraft, while the tail gear, made of nylon plastic, is located approximately 3" from the aft of the plane. In order to allow clearance for the propeller from the ground, a main (front) landing gear strut with a vertical distance 5.5" from the center wheel to the base of the fuselage is used. The wheel diameter for the main landing gear is approximately 2.2". Both the main and tail landing gear are attached to the fuselage through a thin balsa wood layer for structural reinforcement. Two sets of nut and bolt attachments, both at the tail and main gear, will allow the gear to be easily attached and detached for storage purposes.



Figure 4.6.1 Carbon Fiber Main Landing Gear

The structural analysis for the landing gear consisted of modeling both the main and tail landing gear as columns and using the Euler column equation to determine the highest compressive loads during

landing assuming negligible deflection. By establishing a gear load factor¹³ of 3 and multiplying this value by the estimated final weight of the Momma Goose, it was determined that the maximum load on the front gear struts would be approximately 18 lbf, while the tail gear would experience about 9 lbf. Using the material properties for the gear, along with the Euler column equation (see Appendix C), the highest compressive load the front gear can withstand was calculated to be 916 lbf, while the tail gear was calculated to withstand 98 lbf. Both values are clear of the maximum loads that our aircraft will experience.

5. Dynamics and Stability

5.1 Introduction

Analyzing the dynamics and stability of the Momma Goose is essential to successful flight. After performing a conceptual comparison between various tail configurations, our team chose to proceed with a conventional tail instead of a V-tail or T-tail. A conventional tail minimizes the structural rigidity requirement and amount of wiring. Through sizing the tail and control surfaces, static and dynamic stability of the aircraft can be computed.

5.2 Static Stability

Based on historical data, Raymer states that ailerons must extend 50 – 90% of wingspan (113)⁽⁶⁾. Since the wing is constructed in multiple sections, 60% of the wingspan is comprised of the ailerons with

a 5 inch chord without taper. Another source suggests that at least 20 percent of the total wing area must be ailerons to provide roll stability which is satisfied with the dimensions displayed in Table D.1 in Appendix D (Struett, 2012)⁽⁵⁾.

Raymer states that the tail chord should be 50 percent of the wing chord while tail span should be 40 - 50 percent of wingspan (113)⁽⁶⁾. With the 60 inch wingspan and 13.5 inch wing chord, the horizontal tail dimensions are calculated to be at least 28.5 inch span, 7 inch root chord and 5 inch tip chord. Vertical tail span is determined to be 11.5 inches to minimize sideslip effects as seen on the Directional X-plot. An AIAA paper on sizing empennage states that at least 40 percent of vertical tail surface area must be the rudder to have enough yaw stability (Struett, 2012)⁽⁵⁾.

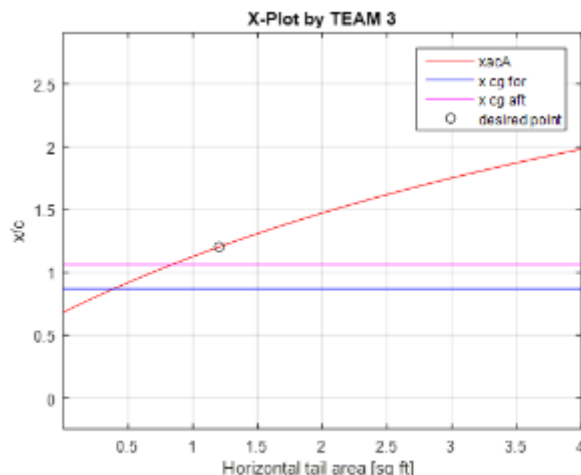


Figure 5.2.1 Longitudinal X-Plot

X-plots shown in Figures 5.2.1 and 5.2.2 validate the Class I sizing based on historical data. The historical data utilized are for general aviation aircraft hence a conservative approach was taken. The dimensions are fairly similar to aircraft built by various senior design teams in the past years.

The vertical tail is sized by the Directional X-plot. As the UAS designed is inherently stable, a feedback system is not required. The Directional X-plot in Figure 5.2.2 yields a $C_{n\beta}$ of 0.006 for a targeted vertical tail area of 0.48 ft². Roskam states that a comparable $C_{n\beta}$ is 0.001. This means that our UAS has more than regular sideslip, but this is necessary to have enough rudder area⁷.

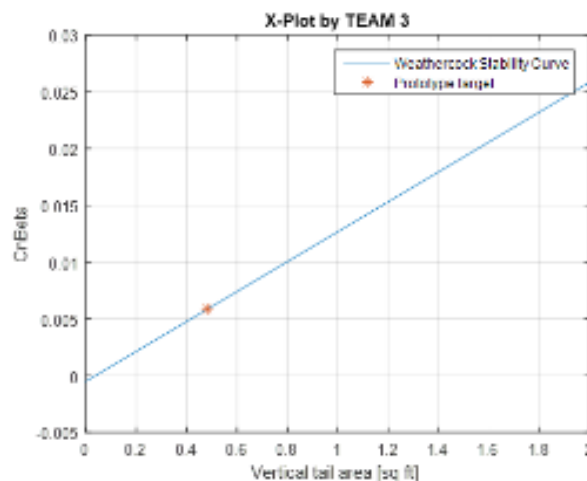


Figure 5.2.2 Directional X-Plot

The Longitudinal X-plot serves to size the horizontal tail area. Note that the static margin indicated by the difference the two lines can change as x_{cg} changes. The desired static margin is 0.20 since Raymer states that typical propeller aircraft have static margin of 0.15. The static margin of .022 shown in Figure 5.2.1 is for a horizontal tail area of 1.2 ft² which is fairly close to the proposed surface area of 1.17 ft².

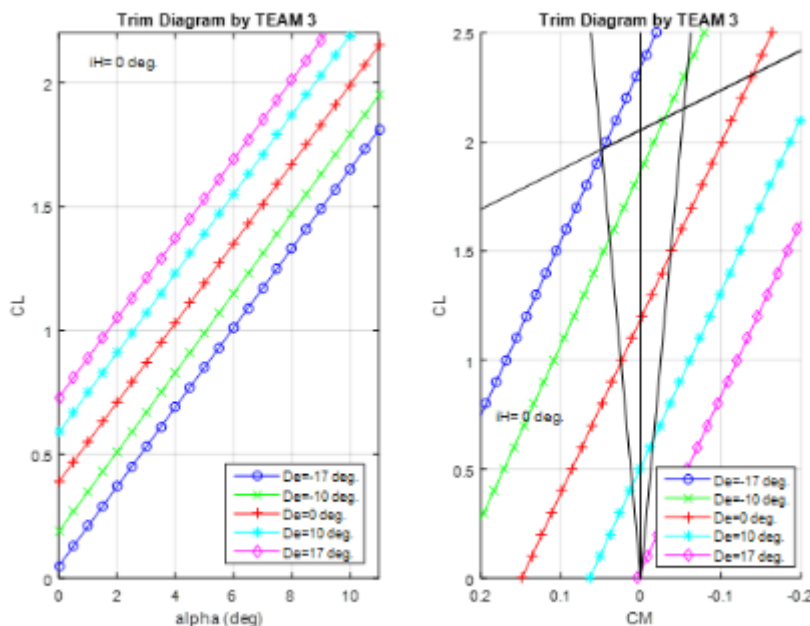


Figure 5.2.3 Trim Diagram

9.35 inches from the datum point, or the nose of the fuselage. This center of gravity is also the forward-limit. In typical aircraft flight, the center of gravity shifts as people/cargo/fuel is expended and moved. In the design aircraft, there is a variable two pound payload that shifts the center of gravity. Without the payload, the aft-limit for the center of gravity is determined to be 11.33 inches.

The second value for determining the static margin of the aircraft is determining the neutral point or aerodynamic center of the aircraft. The governing equation for the neutral point of the aircraft is given from Raymer pg. 417. This analysis deals with a modified equation known as power-off stability. Two terms are neglected in the numerator and denominator that factor in stability changes due to the aircraft's power plant. This is often done to ensure the aircraft's stability is not dictated primarily by the engine. The

center of gravity was determined to be

the aerodynamic center of this aircraft was determined to be located 12.11 inches from the datum point. Figure 5.2.4 shows the location of the aerodynamic center of the aircraft.

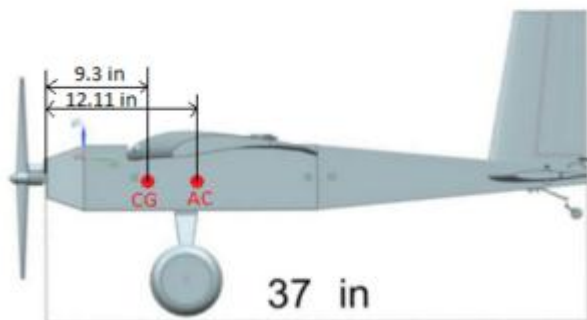


Figure 5.2.4 Location of AC and CG

5%-10% (pg. 417). With the required mission parameters and goal of the design aircraft, the team settled on a desired static margin of 20% (0.20). For the payload-configuration of the aircraft, a static margin of

Upon determining the values indicated in Appendix Table D.1 were satisfactory, the team proceeded to constructing a Trim Diagram. Trim Diagram is used in determining feasible elevator deflections. As seen in Figure 5.2.3, for the given range of center of gravity, the elevators can be deflected -20 to 20 degrees to maintain level flight. Note that the tail airfoil is NACA 0012 to have sufficient cross-sectional area for Servo motors. The stall angle of NACA0012 is also outside of the triangle as required.

The center of gravity was calculated by hand and confirmed by computer analysis. The hand calculations can be seen in Appendix D.7. The design craft's

24.26% was calculated. Without the payload, the static margin shrinks to ~6.9%, which is within acceptable flying limits.

5.3 Dynamic Stability

After determining the aircraft's static stability, its dynamic stability, or stability when performing flight maneuvers or undergoing perturbations during flight, must also be analyzed. Dynamic stability can usually be determined experimentally, however by linearizing the equations of motion a numerical analysis can be performed. This numerical analysis was done using the methods provided in Pamadi⁴.

The first step of this numerical analysis is to determine the stability derivatives in the linear equations of motion. These derivatives were calculated with a MATLAB script that can be found in Appendix (insert appendix here). From these derivatives five modes of stability were calculated.

Mode	Damping Ratio	Natural Frequency (rad/s)
Phugoid Mode	0.71	0.04
Short Period Mode	5.66	0.21
Dutch Roll Mode	0.05	0.6
Roll Subsidence	Time Constant	7.4 seconds
Spiral Mode	Time to Double Amplitude	13 seconds

Table 5.3.1: Stability Modes

From this data the aircraft's handling qualities can be determined. For instance, the short period mode is a heavily damped, high frequency flight perturbation. This will be felt as a strong jolt in the aircraft that will subside quickly and requires no pilot correction to fix.

5.4 Flight Characteristics

With the determined damping ratios and natural frequencies for each of the modes calculated, the flight characteristics and classifications can be determined. These classifications are based upon the data provided in Pamadi⁴.

Mode	Criterion	Value	Classification
Phugoid Mode	$\zeta > 0.04$	0.71	Level I
Short Period Mode	$0.038 < (\omega_n)^2 / (n/\alpha) < 10.0$	0.135	Cat. B Level I
Roll Subsidence	$3.0 < \tau < 10$	7.4	Level III (All Classes)
Dutch Roll Mode	$\omega_n > 0.4$	0.6	Level II (All Categories)
Spiral Mode	$12.0 < \tau$	13	Level II (Category B & C)

Table 5.4.1: Flight Classifications

6. Sense and Avoid

6.1 Introduction

The sense and avoid mission consists of avoiding a balloon hanging 80 ft in the air by at least 50 feet. The balloon will be detected using two sensing tools. A laser based measuring device and a camera. There are two devices being used just in case one does not pick up the balloon correctly. Once sensed, the Momma Goose will indicate to the pilot that there is an obstacle in its flight path. The pilot will then activate the autonomous maneuver and the Momma Goose will avoid the obstacle.

6.2 Conceptual Approach

Our first method utilizes a micro USB camera and a Raspberry Pi microcomputer. The Raspberry Pi will take live video from the camera and utilizing a running MATLAB script, the Raspberry Pi will analyze the images. The script finds the pixels that are moving in the frame and is able to identify them. As the balloon would be moving closer to the camera in frame, range can be calculated. The camera is a widely available model that costs only \$5.00; the Raspberry Pi costs \$40.00. The pi interfaces with the Arduino controller and can issue commands to the servos for autonomous control. The camera will be mounted in the leading edge of the wing and will balance with the Lidar sensor.

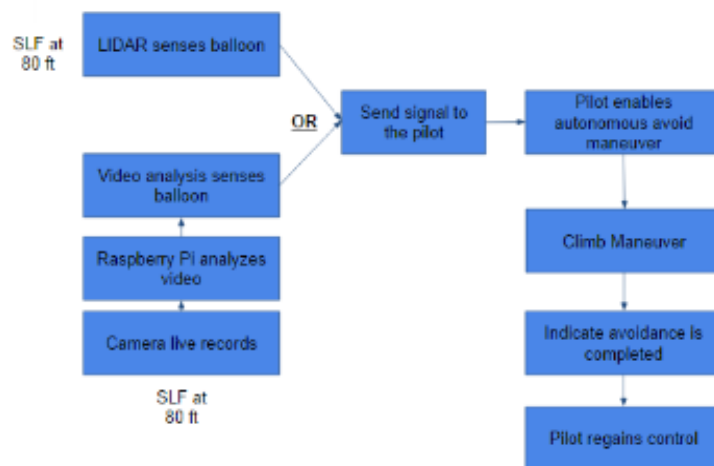


Figure 6.3.1 Flow Chart

This will be very challenging for the pilot and will cause it to miss the balloon. The natural movements of the aircraft does give it movement that may help. This is why two sense and avoid devices are being used in case one does not pick up the balloon. Shown in the flowchart in figure 6.3.1, either the LIDAR or the camera will sense the balloon then send the signal to the pilot.

6.3 Systems Layout and Flow

Figure 3.3.1 shows a flowchart of how the Momma Goose will avoid the balloon. On the camera side, the camera will record what is in front of the Momma Goose live. The Raspberry Pi will analyze the video and measure how far away the objects are. If there is an object within 150 feet, the signal will be sent to the pilot. For the LIDAR, the laser will be measuring 130ft in front of it. If it detects anything a signal will be sent to the pilot. Once the pilot gets the signal, he will activate the autonomous mode. The aircraft will then climb at 45 degrees at full power in order to avoid the balloon by at least fifty feet. Once the Momma Goose has climbed more than 50 feet, it will indicate to the pilot that the avoidance is complete and the pilot will resume flight.

The second sensing equipment being used on the aircraft is a LIDAR-Lite2. This is a small lightweight laser measuring device. It has a range of 40m (130ft), an accuracy of +/- 0.025m, and a weight of 0.04lbs. This is an expensive device with a price around \$115. All of those were retrieved from the Sparkfun website⁸. The location of this device will be in the wing at a distance to offset the weight of the camera on the other wing. It will be inserted into the leading edge similarly to a headlight on commercial aircrafts. A concern with using this device is using it on a moving vehicle. In order for the laser to see the balloon, it will need to line up perfectly in front of the balloon.

6.4 Pilot Acknowledgement

A requirement of the RFP stipulated that the pilot must be notified when the aircraft system senses the presence of an object that it needs to avoid. The Arduino equipped system will send a signal via 2.4 GHz Wi-Fi to a breadboard on the ground with the pilot. A light/buzzer combination will alert the pilot as to the situation of the system and the pilot will then engage the avoidance mode from the controller.

7 Economics

7.1 Cost Breakdown

As stated in the requirements, the team had a \$450.00 budget for the entire prototype fabrication process. Figure 8.1.1 shows the pie chart where WT is wing and tail, SA is sense and avoid, LG is landing gear, P is propulsion and C is control surface associated spending. The pie chart totals to \$408.40. Shipping for all orders was \$6.94 yielding a total of \$415.34.

To minimize spending, the team avoided international shipment requirements. The team also utilized propeller, battery and landing gear available instead of purchasing new items from international warehouses. The costs associated to these items are accounted in the budget as seen in Table F.1 in Appendix F. Although dual sense and avoid sensors increased the spending significantly, the team left over \$30.00 to account of any discrepancies occurring during build process.

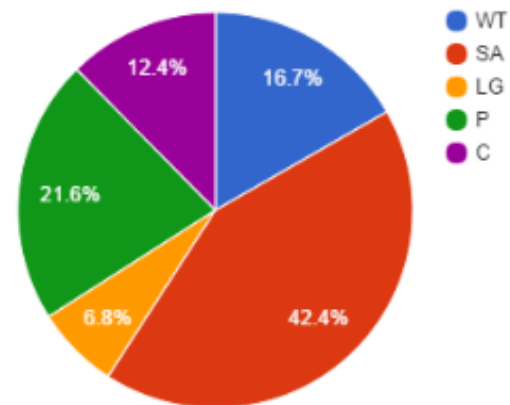


Figure 7.1.1 Budget Distribution

7.2 Schedule and Man Hours

The team kept close tabs on man hours required for each assignment. Figure 8.2.1 shows the total hours spent each week. Weeks 11 through 16 are projected hours based on previous work. The team plans to complete the semester with 1050 man hours. Build process is expected to take 300 hours in three weeks not including glider testing and Arduino projects.

The team plans to build two complete fuselage-wing models to be able to perform testing without high risk. The final prototype is scheduled to be completed by November 19th, 2015 to allow time various full-model ground testing as seen in Appendix F.

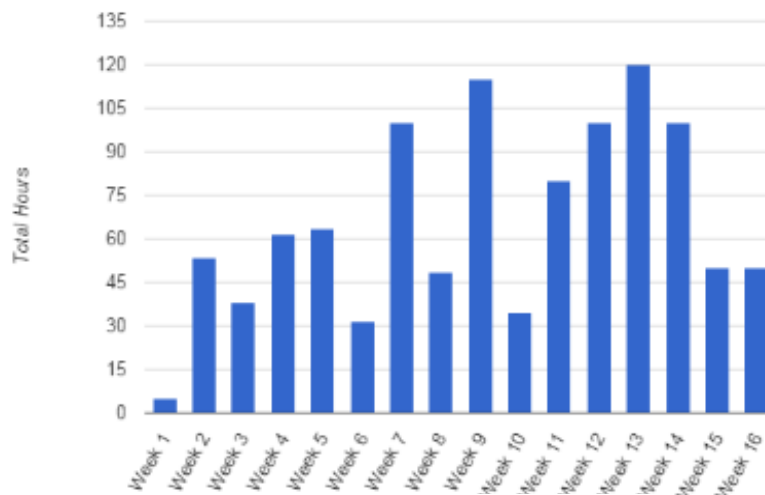


Figure 7.2.1 Total Hours

8 Conclusion

Throughout the development process a test glider was built concurrently. This test glider provided a means of testing theoretical design concepts that would or would not be applied to the final design aircraft. This test glider provided a means for experimental data to be gathered and not rely entirely on numerical and theoretical analysis.

Theoretically, our aircraft has a maximum turn rate of 162.6 degrees per second and a minimum turn radius of 11.3 feet. These specifications allow the aircraft to successfully avoid the balloon in the sense



and avoid mission. The aircraft has a thrust cruise of 1.037 lbf and a thrust takeoff of 1.2 lbf. The cruise velocity of 27 feet per second. The cruise lift coefficient is 1.22. The maximum flight velocity

Figure 8.1 Test Glider

(propeller limited) is 36 feet per second. The total propulsive efficiency (including the propeller, motor, and battery) is 0.5.

The flight endurance is 14 minutes at an ambient temperature of 59 degrees Fahrenheit, and 12 minutes at 32 degrees Fahrenheit. Assuming the ambient flight temperatures are in acceptable range, the aircraft will be able to achieve its desired flight endurance of 12 minutes at the required altitude of 200-300 feet. The max cruise flight path angle is 36 degrees and the max takeoff flight path angle is 62 degrees, giving the aircraft a climb angle of greater than 25 degrees. The aircraft will be able to abort takeoff at approximately 40 feet based upon the velocity being lower than the minimum flight velocity. Based upon the minimum flight velocity the aircraft will achieve takeoff between 45-50 feet, which meets the RFP requirements. The final proposed budget of the aircraft is \$408.40, which keeps the aircraft under the maximum budget of \$450.00.

The aircraft has been designed to achieve a minimum assembly time in under 10 minutes. The aircraft remains dynamically stable with a variety of payload weights and batteries, and the tail-dragger configuration prevents any damage to the aircraft by the runway during takeoff or landing. A majority of the flight characteristics give the aircraft and overall acceptable flight qualities and should demonstrate ample stability for the average pilot. The sense and avoid technology has demonstrated its capabilities and should continue this effectiveness into the field.

Furthermore, figure 8.1 demonstrates that all components of the aircraft will fit within the designated box provided to all teams. This completes the RFP requirements and ensures the aircraft will achieve its design goals.

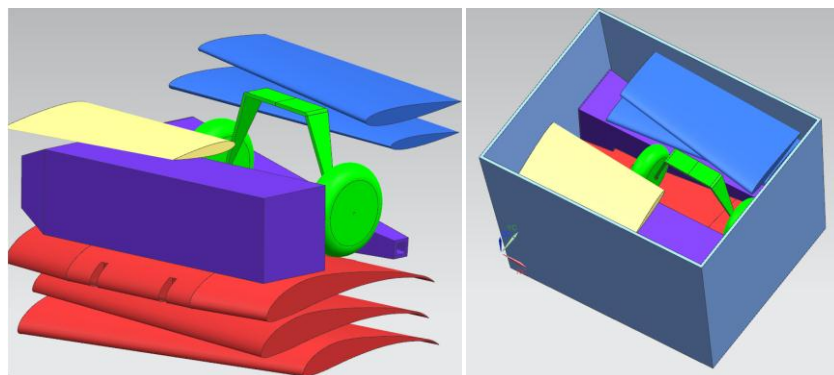


Figure 8.2: Aircraft Components in box

9 References

- {1} Lissman, “Low-Reynolds-Number Airfoils,” Annual Review of Fluid Mechanics, published online Jan. 1983; Vol. 15: pp.223-239. DOI: 10.1146/annurev.fl.15.010183.001255
- {2} “APC Performance Data Files” APC Propellers Dec 21, 2014.
https://www.apcprop.com/v/PERFILES_WEB/listDatafiles.asp
- {3} Dr. Andrisani, Main_System_Design, Purdue University
- {4} Pamadi, Bandu N., *Performance, Stability, Dynamics, And Control of Airplanes*, 2nd Edition, AIAA Education Series
- {5} Struett, Ryan C., “Empennage Sizing and Aircraft Stability using MATLAB.” AIAA Paper, Jun. 2012.
- {6} Raymer, Dan, *Aircraft Design: A Conceptual Approach*, AIAA Education Series.
- {7} Roskam, Dr. Jan, *Airplane Design, Volumes I-VIII*
- {8} “LIDAR Lite 2”. Sparkfun. Retrived
from: <https://www.sparkfun.com/products/13680?gclid=CPPvjM6Hs8gCFQkxaQod2SsNxA>
- {9} “The Original K&J Magnet Calculator,” *K&J Magnetics*,
<https://www.kjmagnetics.com/calculator.asp> [retrieved 20 October 2015]
- {10} “Physical Properties of Extended Polystyrene,” *Northwest Foam Products, Inc.*, Twin Falls, ID, 2007, <http://www.northwestfoam.com/fact-specs.htm> [retrieved 20 October 2015]
- {11} “Fiberglass,” *ACP Composites*, Livermore, CA, 2010, <http://www.acpsales.com/Fiberglass.html> [retrieved 20 October 2015]
- {12} “Mechanical Properties of Materials,” *Performance Composites, Ltd.*, 2009,
<http://www.performance-composites.com/> [retrieved 28 October 2015]
- {13} Raymer, Dan, *Aircraft Design: A Conceptual Approach*, AIAA Education Series.

Appendix A – Aerodynamics

A.1 Figures

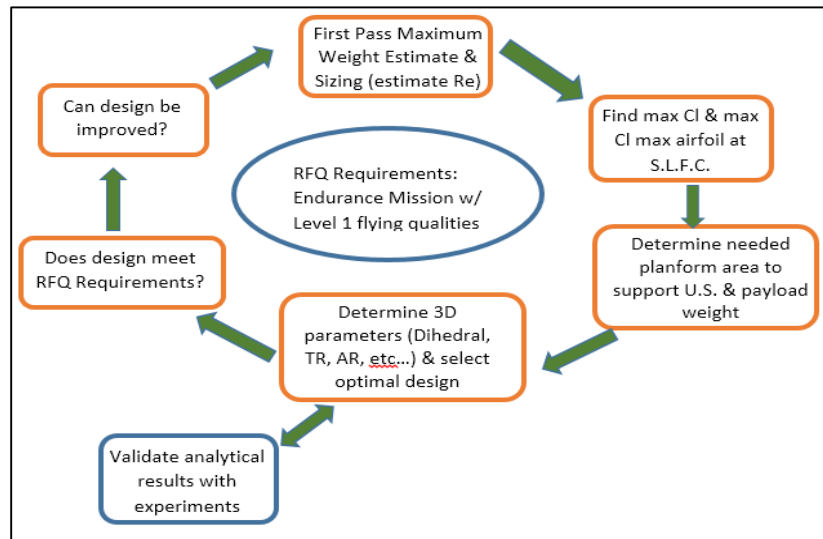


Figure A.1: Team 3 Aerodynamic Design Process

A.2 Equations

$$L = (.5 * \rho * S * C_l * V_{\infty}^2) / g$$

Equation 1: Lift Equation

Where:

ρ = Freestream Flow Density (lbm/ft³)

C_l = Coefficient of Lift

S = Wing Planform Surface Area (ft²)

V_{∞} = Freestream Flow Velocity (ft/s)

g = Gravitational Constant

A.3 Code

Below is the MATLAB code that was utilized to develop the constraint diagram given in Figure 2.6.

```

%%Aaron Lemcherfi
%%AAE 451

%Constraint Diagram Analysis
%Note: Takeoff constraint is not shown on plot for simplicity due to the fact
that other constraints posed by our RFP are significantly more restrictive on
our design space

close all
clear all
clc

%% Constants
rho_english = 0.0765; %Air density (lbm/ft3)
Eta_P = .7; %Propeller Efficiency
V_cr_mph = 22; %Cruise Velocity (mph)
V_cr_FtperSec = 24 %Cruise Velocity (ft/s)
V_stall = 23; %Stall Velocity (ft/s)
  
```

```

    S = 4.9; %Wing Surface Area
    (ft^2)
    gamma = 37.5*pi/180; %Climb Angle (deg)
    PrcntPower_Cr = .75; %Percent of Power Used @
Cruise
    CL = 1.1; %Lift Coefficient
    L_over_D = 8;
    CD = .11; %Drag Coefficient
    CD1 = 1.1*.11; %Drag Coefficient

%% Stall Speed Requirement Constraint
    CLmax = 1.6;
    while CLmax <= 2.2
        W_over_S = (.5 * rho_english * V_stall^2 * CLmax) /
32.17;
        W_over_S_plot = linspace(W_over_S,W_over_S,100);
        PowerLoadingRange = linspace(0,100,100);
        plot(W_over_S_plot,PowerLoadingRange,'--')
        hold on
        CLmax = CLmax + .2;
    end
%% Cruise Speed Requirement Constraint
    WingLoading = linspace(0,1.25,1000);
    W_over_SHP = (32.2*550*Eta_P / (.5 * rho_english *
V_cr_FtperSec^3 * CD)) * WingLoading;
    plot(WingLoading,W_over_SHP,'--')
    hold on
    W_over_SHP1 = (32.2*550*Eta_P / (.5 * rho_english *
V_cr_FtperSec^3 * CD1)) * WingLoading;
    plot(WingLoading,W_over_SHP1)
    hold on
%% Climb Angle Requirement Constraint
    L_over_D_max1 = linspace(8,8,1000);
    L_over_D_max2 = linspace(10,10,1000);
    L_over_D_max3 = linspace(12,12,1000);
    L_over_D_max4 = linspace(12,14,1000);
    W_over_Power1 =
550*Eta_P./(V_cr_FtperSec.*((1./(.866*L_over_D_max1))+sin(gamma))
);
    W_over_Power2=
550*Eta_P./(V_cr_FtperSec.*((1./(.866*L_over_D_max2))+sin(gamma))
);
    W_over_Power3 =
550*Eta_P./(V_cr_FtperSec.*((1./(.866*L_over_D_max3))+sin(gamma))
);
    W_over_Power4 =
550*Eta_P./(V_cr_FtperSec.*((1./(.866*L_over_D_max3))+sin(gamma))
);
    XLine = linspace(0,1.5,1000);
    Lover_D1 = plot(XLine,W_over_Power1,'b');
    hold on
    set(Lover_D1,'Markersize',1);
    Lover_D2 = plot(XLine,W_over_Power2,'r');
    hold on
    set(Lover_D2,'Markersize',1);

```

```

    Lover_D3 = plot(XLine,W_over_Power3,'g');
    hold on
    Lover_D4 = plot(XLine,W_over_Power4,'g');
    hold on
    set(Lover_D3,'Markersize',1);

%% Plot Results
    title('Constraint Diagram')
    ylabel('W/P: (Aircraft Weight / Power) [lbf/hp]');
    xlabel('W/S: (Aircraft Wight[lbf] / Wing Planform Surface
Area[ft^2])')
    grid on
    axis([.1 1.5 0 100])
    legend('Stall Speed: CLmax = 1.6','Stall Speed: CLmax = 1.8',...
        'Stall Speed: CLmax = 2.0', 'Stall Speed: CLmax =
2.2','Cruise Speed: CD=0.122','Cruise Speed: CD=0.13',...
        'Climb Angle: (L/D)max = 8','Climb Angle: (L/D)max = 10',...
        'Climb Angle: (L/D)max = 12','Climb Angle: (L/D)max =
14','Take-off Constraint');

```

Appendix B – Propulsion System

B.1 Code

```
Dr. Andrisani Main_System_Design
clear
clear functions
close all
ifig=0;
hold off
disp(' '); disp('>>> Start of script. <<<'); disp(' ')
echo on
% Script to design an end-to-end propulsion system for an
% electric-powered propeller-driven aircraft.
% Given:
%   drag polar,
%   aircraft weight, air density,
%   pitch to diameter ratio of the prop and prop data,
%   motor constants for a particular motor.
%
% Find:
%   speed for maximum endurance,
%   propeller diameter,
%   gear ratio,
%   voltage at which to operate the motor,
%   battery sizes to achieve the desired battery voltage,
%   endurance for single strand and dual strand batteries,
%   for an aircraft flying straight and level or turning with a
%   specified turn radius.
%
% PHASE 1: AIRCRAFT SUBSYSTEM
%
% This data is roughly for the Boiler Express Aircraft
CD0=.0480; % drag coefficient when CL=0.
S= 4.3;    % wing area
A=(57/12)^2/S; % aspect ratio span squared divided by reference area
e=.75; % Oswalds efficiency factor
V=10:1:40; % velocity in ft/sec
rho=.002377; % air density in slugs/ft^3
W= 6;      % aircraft weight in pounds (lbf)
R=50;      % Radius of steady turn (ft)
echo off
[Pop,Vop,EtaAircraft,Pre,Ve,ifig]=DesignAircraft2(W,rho,S,CD0,A,e,V,ifig,R);
%
% PHASE 2: PROPELLER SUBSYSTEM
%
% Define hypothetical propeller for specified p/D=.857
string1=['Data for hypothetical propeller with tau=p/D=.857'];
disp(string1);
echo on
tau=12/14;
J = [    0.3100    0.3900    0.5100    0.6200 0.7000    0.8200];
CT = [    0.1109    0.1100    0.1046    0.0929 0.0815    0.0610];
CP = [    0.0720    0.0756    0.0784    0.0764 0.0716    0.0597];
echo off
[Jstar,CTstar,CPstar,Etastar,ifig]=PlotProp(J,CT,CP,string1,ifig);
% Propeller power equals the operating power of the aircraft
```

```

% The propeller is operating at a forward speed given by Vop
% Find the required propeller diameter
[Dactual,Jactual,nactual,RPMactual,EtaPropactual,Poutactual,Ppinactual,ifig]=
...
DesignProp(rho,Pop,Vop,Jstar,CTstar,CPstar,Etastar,J,CT,CP,ifig); % <<< lots
of work here
RPMprop=RPMactual;
PinPropWatts=Ppinactual*1.356; % convert to watts from ft-lbf/sec
PlotProp2(Jactual,EtaPropactual,J,CT,CP,ifig);
Pitch=tau*Dactual*12;
string2=[' You have selected a ',num2str(Dactual*12),'x',num2str(Pitch),'
prop.'];
disp(string2); disp(' ');
function
[Pop,Vop,EtaAircraft,Pre,Ve,ifig]=DesignAircraft2(W,rho,S,CD0,A,e,V,ifig,R)
% function
[Pop,Vop,EtaAircraft,Pre,Ve,ifig]=DesignAircraft2(W,rho,S,CD0,A,e,V,ifig,R)
% This version designs for a steady turn with radius of turn equal to
% R=50 feet.
% OUPUTS
% Pop is operating power of the aircraft (ft-lbf/sec)
% Vop is the operating velocity of the aircraft (ft/sec)
% Pre is the minimum poewr required (ft-lbf/sec)
% Ve is the velocity of the aircraft for minimum power required (ft/sec)
%
% INPUTS
% CD0= drag coefficient when CL=0.
% A= aspect ratio span squared divided by reference area
% e= Oswalds efficiency factor
% V= velocity vector in ft/sec
% rho= air density in slugs/ft^3
% W= aircraft weight in pounds (lbf)
% S= wing area
% ifig is the figure number of the plot
% R aircraft turn radius (feet)
tanphi=(V.*V)/(32.17*R); %tangent of bank angle Roskam eqn 4.89
phirad=atan(tanphi); % bank angle, radians
n=1./cos(phirad); % load factor, g, Roskam eqn 4.92
k=1/(pi*A*e); % k from the drag polar CD=CD0+k*CL^2
CL=2*n*W./(rho*S*V.*V); % Lift coefficient as a function of velocity
CD=CD0+k*CL.*CL; % Drag coefficient as a function of velocity
ifig=ifig+1;
figure(ifig);
subplot(311); plot(V,phirad*180/pi)
ylabel('Bank angle, phi (deg)')
string40=['Steady turn with turn radius of ',num2str(R),' ft'];
title(string40)
subplot(312); plot(V,n)
ylabel('Load factor n (g)')
subplot(313); plot(V,CL)
ylabel('Lift coefficient')
xlabel('Velocity (ft/sec)')
Pr=.5*rho*S*V.^3.*CD; % Power required ft/lbf/sec
ifig=ifig+1;
figure(ifig); plot(V,Pr)
xlabel('Velocity (ft/sec)')
ylabel('Power required (ft-lbf/sec)')

```



```

string41=['Aircraft Power required vs trim speed for a turn radius of
',num2str(R),' ft'];
title(string41)
%CLe=sqrt(3*CD0/k); % Lift coefficient for maximum endurance (minimum power
required)
%CDe=4*CD0; % Drag coefficient for maximum endurance (minimum power required)
%Ve= sqrt(2*W/(rho*S*CLe)); % Speed for maximum endurance (minimum power
required)
%Pre=interp1(V,Pr,Ve); % YI = INTERP1(X,Y,XI) % minimum power
required
ipre=find(Pr==min(Pr));
Pre=Pr(ipre);
Ve=V(ipre);
tanphie=(Ve*Ve)/(32.17*R); %tangent of bank angle Roskam eqn 4.89
phirade=atan(tanphie); % bank angle, radians
ne=1/cos(phirade); % load factor, g, Roskam eqn 4.92
CLe=2*ne*W/(rho*S*Ve*Ve);
hold on
plot([Ve,Ve],[0,Pre],':'); plot([0,Ve],[Pre,Pre],':')
string1=['Minimum power of ',num2str(Pre),' ft-lbf/sec is achieved at a speed
of ',num2str(Ve),' ft/sec.'];
string1a=['The lift coefficient at this minimum power condition is
',num2str(CLe),'.'];
disp(' '); disp(string1);
text(5,Pre-1,string1)
text(5,Pre-4,string1a)
hold off
VopInput=input('At what speed would you like to operate the aircraft?
Default=Ve (speed for min. power required) >>>>');
if isempty(VopInput)
    Vop=Ve;
    Pop=Pre;
    CLoP=CLe;
else
    Vop=VopInput;

    tanphiop=(Vop*Vop)/(32.17*R); % bank angle Roskam eqn 4.89
    phiradop=atan(tanphiop); % bank angle
    nop=1./cos(phiradop); % load factor Roskam eqn 4.92
    CLoP=2*nop*W./(rho*S*Vop*Vop); % Lift coefficient as a function of
velocity
    CDop=CD0+k*CLop.*CLop; % Drag coefficient as a function of velocity
    Pop=.5*rho*S*Vop^3.*CDop; % Power required ft/lbf/sec
    hold on
    plot([Vop,Vop],[0,Pop],':'); plot([0,Vop],[Pop,Pop],':');
    string3=['Operating power of ',num2str(Pop),' ft-lbf/sec is required at
an operating speed of ',num2str(Vop),' ft/sec'];
    text(5,Pop+1,string3)
    hold off
end
disp(' '); disp('AIRCRAFT SUMMARY');
string2=[' You are asking the Propeller to deliver ',num2str(Pop),' ft-
lbf/sec of power at a speed of ',num2str(Vop),' ft/sec.'];
EtaAircraft=Pre/Pop;
string4=['The operating efficiency of your aircraft is
',num2str(EtaAircraft)];
disp(string2); disp(string4);

```

```

hold on; text(5,Pop+3,string4);
string1c=['The operating lift coefficient at this condition is
',num2str(CLop),'.'];
text(5,Pop+5,string1c)
hold off
disp(string1c)
disp('Is your wing capable of generating this much lift coefficient, and do
you have adequate stall margin?')
disp(' ');
function [Jstar,CTstar,CPstar,Etastar,ifig]=PlotProp(J,CT,CP,string1,ifig)
ifig=ifig+1;
figure(ifig)
Eta=CT.*J./CP;
subplot(311); plot(J,CT); grid
ylabel('Thrust Coef, CT')
title(string1)
subplot(312); plot(J,CP); grid
ylabel('Power Coef, CP')
subplot(313); plot(J,Eta); grid
ylabel('Efficiency, eta')
xlabel('Advance ratio, J=V/(nD)')
j=find(Eta==max(Eta));
Jstar=J(j);
CTstar=CT(j);
CPstar=CP(j);
Etastar=CTstar.*Jstar./CPstar;
subplot(311); hold on;
plot([Jstar,Jstar],[0,CTstar],'r:',[0,Jstar],[CTstar,CTstar],'');
string2=['CT*= ',num2str(CTstar),' for J*= ',num2str(Jstar)];
text(.1,CTstar+.006,string2)
hold off
subplot(312); hold on;
plot([Jstar,Jstar],[0,CPstar],'r:',[0,Jstar],[CPstar,CPstar],'');
string3=['CP*= ',num2str(CPstar),' for J*= ',num2str(Jstar)];
text(.1,CPstar+.005,string3)
hold off
subplot(313); hold on;
plot([Jstar,Jstar],[0,Etastar],'r:',[0,Jstar],[Etastar,Etastar],'');
string3=['Eta*= ',num2str(Etastar),' for J*= ',num2str(Jstar)];
text(.1,Etastar-.1,string3)
hold off
function
[Dactual,Jactual,nactual,RPMactual,Etaactual,Poutactual,Ppinactual,ifig]=...
DesignProp(rho,Pop,Vop,Jstar,CTstar,CPstar,Etastar,J,CT,CP,ifig)
Dstar=sqrt(Pop/(Vop*rho*CTstar*(Vop/Jstar)^2)); % Propeller diameter (ft)
Dstarinches=Dstar*12; % Propeller diameter (inches)
nstar=Vop/(Jstar*Dstar); % propeller speed (Hz)
RPMstar=nstar*60; % Propeller revolutions per minute
disp(' '); disp('PRELIMINARY PROPELLER ANALYSIS');
string2=[' If the propeller of diameter ',num2str(Dstarinches),' inches'];
string3=[' spins at ',num2str(RPMstar),' rpm,'];
string4=[' the propeller efficiency will be maximum at Eta*=
',num2str(Etastar),',,'];
string5=[' at the airspeed of ',num2str(Vop),' ft/sec,'];
string6=[' and the prop will be generating the required ',num2str(Pop),' ft-
lbf/sec of power.'];
disp([string2,string3]);disp(string4);disp(string5);disp(string6),disp(' ');

```

```

Dinches=input('What propeller diameter in inches do you want to use?
Default=D* >>>');
if isempty(Dinches)
    Dactual=Dstar; % Actual prop diameter is the one for maximum efficiency
    (ft)
    Jactual=Jstar; % Actual propeller advance ratio
    Poutactual=Pop; % Actual propeller power, ft-lbf/sec
    nactual=nstar; % Actual propeller frequency, Hz
    RPMactual=nactual*60; % Actual propeller RPM
    Etaactual=Etastar; % Actual propeller efficiency
    Ppinactual=rho*nactual^3*Dactual^5*CPstar; % Propeller input power (from
shaft) ft-lbf/sec
else
    Dactual=Dinches/12; % Actual diameter is the manually input one converted
to ft.
    nj=length(J);
    Pprop(2:nj)=Vop*rho*(Vop./(J(2:nj)*Dactual)).^2*Dactual^4.*CT(2:nj);
    %ifig=ifig+1; figure(ifig); plot(J(2:nj),Pprop(2:nj));
xlabel('J');ylabel('Propeller power ft-lf/sec')
    %string7=['Propeller power as a function of J for the prop of
',num2str(Dinches),' inches.'];
    %title(string7)

    %YI = INTERP1(X,Y,XI)
    Jactual=interp1(Pprop(2:nj),J(2:nj),Pop); % Actual propeller advance
ratio
    Poutactual=interp1(J,Pprop,Jactual); % Actual propeller power, ft-lbf/sec
    nactual=Vop/(Jactual*Dactual); % Actual propeller frequency, Hz
    RPMactual=nactual*60; % Actual propeller RPM
    %hold on
    %plot([Jactual,Jactual],[0,Poutactual],'r',[J(2),Jactual],[Poutactual,Po
utactual],':')
    %hold off
    CPoutactual=interp1(J,CP,Jactual);
    Ppinactual=rho*nactual^3*Dactual^5*CPoutactual; % Propeller input power
(from shaft) ft-lbf/sec
    CTactual=interp1(J,CT,Jactual);
    Poutactual2=Vop*rho*nactual^2*Dactual^4*CTactual;
    %Etaactual3=Poutactual/Ppinactual;
    %Etaactual2=Poutactual2/Ppinactual;
    Etaactual=interp1(J,CT.*J./CP,Jactual);
end
disp(' '); disp('PROPELLER SUMMARY')
string8=[' A propeller of ',num2str(Dactual*12),' inches'];
string9=[' spinning at ',num2str(RPMactual),' RPM at a translational speed
of ',num2str(Vop),' ft/sec'];
string10=[' produces an output power of ',num2str(Poutactual),' ft-
lbf/sec,'];
string10a=[' has an efficiency of ',num2str(Etaactual),','];
string11=[' and absorbes an input power of ',num2str(Ppinactual),' ft-
lbf/sec or ',num2str(Ppinactual/550),' HP.'];
disp(string8); disp(string9); disp(string10); disp(string10a);
disp(string11);

```

Appendix C – Weights and Structures

Total Weight Determination and Center of Gravity

Early in the developmental and design stages, our team used historical AIAA data and our battery weight fraction to establish a weight estimate for the Momma Goose. This estimate, though low compared to our final weight, provided us with a starting point and goal to aim for in our design. The code used for the estimate is shown below. The graph output showing the estimated weight is shown in Figure C.1

```
%%%%%%%%%%%%%%%%%%%%%%%%%%%%%%%%%%%%%%%%%%%%%%%%%%%%%%%%%%%%%%%%%%%%%%%%%
% Weight Estimation Code
% W. Sarmiento
%%%%%%%%%%%%%%%%%%%%%%%%%%%%%%%%%%%%%%%%%%%%%%%%%%%%%%%%%%%%%%%%%%%%%%%%%
clear all
close all
clc

% Variables
n_m = .7; % efficiency of motor
n_p = .65; % efficiency of propeller
P_m = 137.5; % power of motor [ft*lb/sec]
P_p = P_m * n_p * 4.44*.3; % Prop power [m*N/sec]
V_stall = 6.7; % [m/s]
V_lf = V_stall*1.2; % velocity at level flight [m/s]
V_tu = V_stall*1.3; % velocity at turning [m/s]
V_cl = V_stall*1.2; % velocity at climb [m/s]
T_lf = 1.3*4.44; % thrust at level flight [N] | .066 in lbf
T_tu = 1.3*4.44; % thrust for turning flight [N]
T_cl = 1.64*4.44; % thrust for climb [N]
T_to = 1.64*4.44; % thrust for take-off [N]
L_D = 8; % lift/drag ratio
rho_b = 230000/4.44; % energy density of the battery [joules/N]
gamma = 25; % flight path angle [deg]
w_p = 2; % payload weight [lb]

% Power Calculations
P_b = P_p/(n_p*n_m); %Battery Power [m*N/sec]

% Battery Weight Fractions for individual flight sections
W_b_lf = (1.356*V_lf*T_lf)/(L_D*n_p*n_m*rho_b); % at level flight
W_b_tu = (1.356*V_tu*T_tu)/(L_D*n_p*n_m*rho_b); % for turning flight
W_b_cl = (1.356)/(n_p*n_m*rho_b) *...
    V_cl*T_cl*(cosd(gamma)/(L_D)+sind(gamma)); % for climb
W_b_to = (745.7*T_to)/(L_D*n_m*rho_b); % for take-off
W_b_to = .002;
W_b_wu = 10*W_b_to; % for warm up

% Total weight battery fraction
W_b = W_b_to + W_b_wu + W_b_cl + W_b_lf + W_b_tu;

% Plot
w = 0:0.1:15;
battery_pay = W_b.*w + w_p;
hist_data = 0.2647.*w + .8559;
```

```

plot(w,battery_pay,'b');
hold on
plot(w,hist_data,'r');
title('Weight Estimation using Historical Weight Data')
xlabel('Weight [lbf]')
ylabel('W-W_e and W_b+Wp [lbf]')
legend('Estimated Weight','Historical Data')

% References
% http://personal.osi.hu/fuzesisz/strc\_eng/
% http://propellerhub.com/measuring-pitch.html
%%%%%%%%%%%%%%%%%%%%%%%%%%%%%%%%%%%%%%%%%%%%%%%%%%%%%%%%%%%%%%%%%%%%%%%%

```

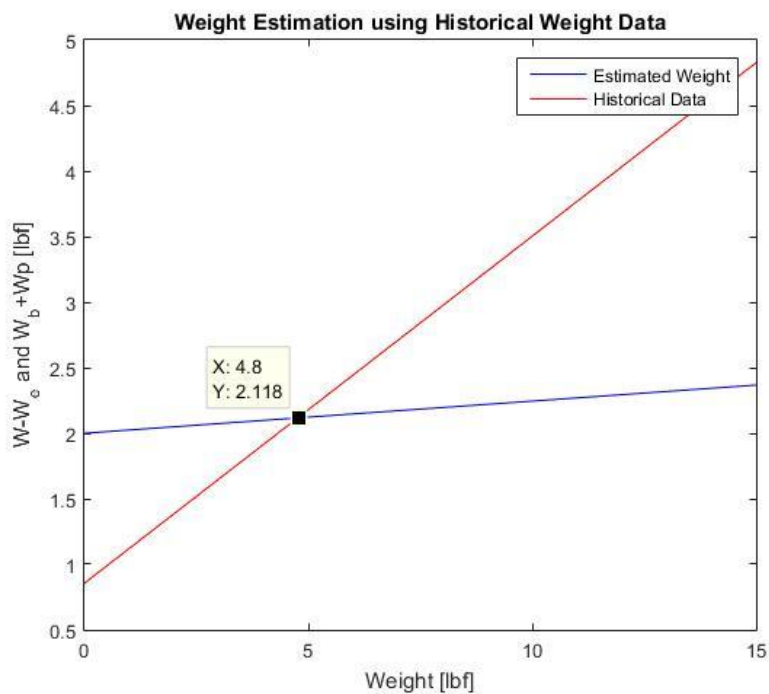


Figure C.1 Weight Estimation using Historical Weight Data

Once we had a fully developed design, each component of the aircraft was individually taken, weighed, and measured to see how far they were located from the nose of the Momma Goose. This enabled our team to calculate a total weight of 5.98 lbs and center of gravity of 9.35” from the nose of the aircraft. This data is shown in table C.1.

COMPONENT	W (grams)	W_n/W_0	x (in from nose)	$(W_n/W_0)*x$
Propeller	37.99	0.014	-1.7	-0.02
Motor	57.00	0.021	0.8	0.02
Battery	331.82	0.122	4.0	0.49

Servo Group Tail	74.00	0.027	36.0	0.98
Servo Group Wing	74.00	0.027	17.0	0.46
Gearbox	39.00	0.014	0.6	0.01
Speed controller	25.00	0.009	4.5	0.04
Front landing gear	36.00	0.013	10.0	0.13
Rear landing gear	18.00	0.007	34.0	0.23
Payload	907.19	0.334	5.4	1.80
Rubber Bands	11.34	0.004	15.0	0.06
Fuselage	100.00	0.037	17.0	0.63
Wing	664.06	0.244	10.0	2.44
Tail	61.36	0.023	32.0	0.72
Magnets (front 1)	5.27	0.002	11.0	0.02
Magnets (front 2)	5.27	0.002	13.0	0.03
Magnets (rear)	5.27	0.002	44.0	0.09
Carbon Fiber Rods	28.67	0.011	10.0	0.11
CF Rods Tail	14.33	0.005	32.0	0.17
Rubber Band Rod 1	7.71	0.003	6.1	0.02
Rubber Band Rod 2	7.71	0.003	18.0	0.05
Rubber Band Rod 3	7.71	0.003	19.6	0.06
Rasppi	45.00	0.017	9.0	0.15
Lidar	26.50	0.010	8.0	0.08
Camera	22.68	0.008	8.0	0.07
arduino	25	0.009	14.5	0.13
screws front	50.00	0.018	10	0.18
screws back	15.00	0.006	34	0.19
Prop Plate	5.44	0.002	0.1	0.00
Front Plate	10.00	0.004	10	0.04
Back Plate	0.20	0.000	34	0.00
TOTAL	2718.51	1.000		9.35
WEIGHT (lbs)	5.98		C.G.	9.35

Table C.1 Weight Determination and Center of Gravity

Wing Magnet Analysis

In order to determine the total pull force from our magnets, a website named K&J Magnetics⁹, provided an accurate tool that outputted the distance and total pull force from magnet to magnet connection. The input parameters for the analysis included the following:

- Magnet grade: N48
- Diameter: 0.25"
- Thickness: 0.0625"
- Distance (in between magnets): 0"

The analysis showed a resulting force of 1.36 lbf per magnet connection. Figure C.2 shows a plot of pull force (in lbs.) versus the distance between the magnets.

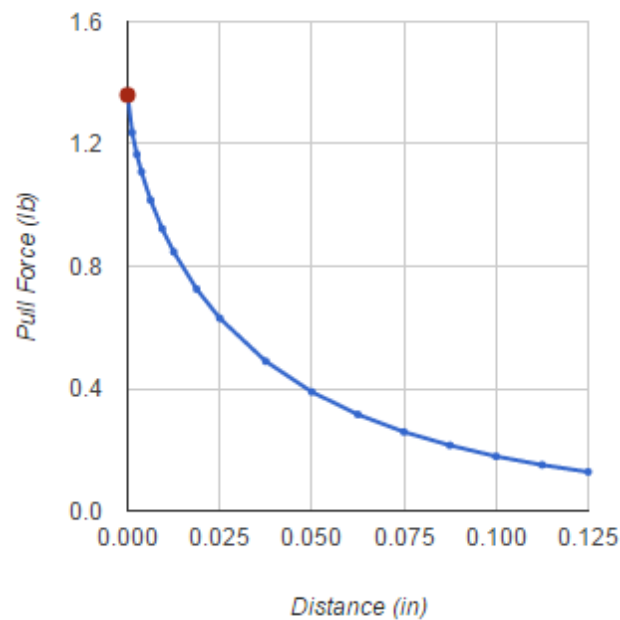


Figure C.2 Pull Force vs. Distance for N48 Magnet⁹

Code and Calculations for Analysis of Wing Bending Moment

```
%%%%%%%%%%%%%%%%%%%%%%%%%%%%%%%%%%%%%%%%%%%%%%%%%%%%%%%%%%%%%%%%%%%%%%%%%
% Wing Load Distribution Code
% W. Sarmiento
%%%%%%%%%%%%%%%%%%%%%%%%%%%%%%%%%%%%%%%%%%%%%%%%%%%%%%%%%%%%%%%%%%%%%%%%%
close all
clear all
clc

% Inputs
L_max = 13.3;           % max lift force [lbf]
```



```

b = 57; %wing span [in]
x = 0:1:(b/2); %distance along wing [in]
M = L_max.*(x.^2)./(2*b); %bending moments [in-lbf]
x_flip = (b/2):-1:0;

% Plots
% Bending moment
bar(x_flip,M)
xlabel('Distance from Fuselage [in]')
ylabel('Bending Moment [in-lbf]')
title('Bending Moment Distribution')
%%%%%%%%%%%%%%%%%%%%%%%%%%%%%%%%%%%%%%%%%%%%%%%%%%%%%%%%%%%%%%%%%%%%%%%%

```

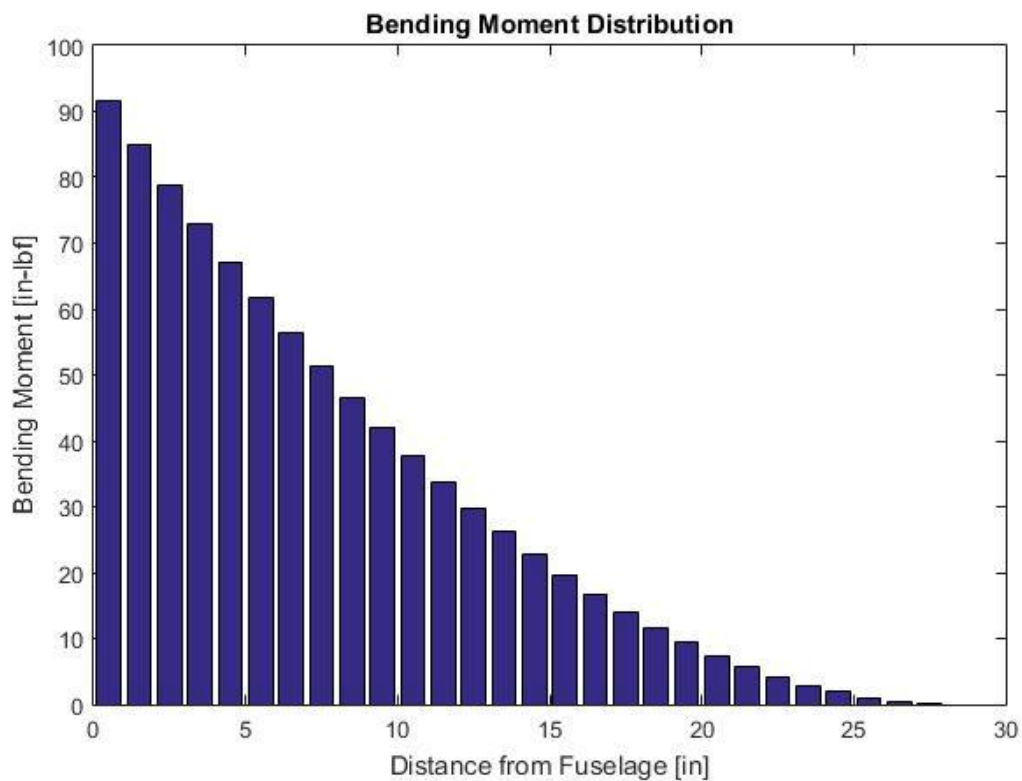


Figure C.2 Bending Moment Distribution

Code and Calculations for Fiberglass Thickness

Assumptions for bending moment analysis for fiberglass thickness are listed as follows.

- Rectangular Lift
- Airfoil Modeled as rectangle
- Fiberglass skin takes all load

$$\phi = \tan^{-1} \frac{V^2}{r * g} = 48.36^\circ$$

The calculated assumptions are:

- V for turning = ~30 feet/sec
- Turning radius (r) of 25 feet
- Weight = 6 lbs
- g = 32 feet/sec²

$$n = \frac{1}{\cos(\phi)} = 1.5 \rightarrow (x 1.5) = 2.25$$

$$L_{max} = n * W = 13.3 \text{ lbf}$$

```
%%%%%%%%%%%%%%%%%%%%%%%%%%%%%%%%%%%%%%%%%%%%%%%%%%%%%%%%%%%%%%%%%%%%%%%%
% Wing Load Calculations Code
% W. Sarmiento
%%%%%%%%%%%%%%%%%%%%%%%%%%%%%%%%%%%%%%%%%%%%%%%%%%%%%%%%%%%%%%%%%%%%%%%%
close all
clear all
clc

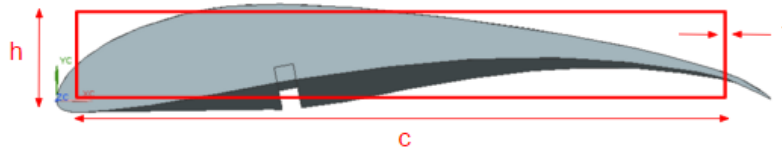
% LOAD FROM BENDING
% Variables
V = 30; %ft/sec
r = 25; %ft
g = 32; %ft/sec^2
W = 5.88; % weight of aircraft
fiber_comp = 9.94e6; % [lb/ft^2]
c = 1.083; % [ft]
h = .125; % [ft]

%Calculations thickness
phi = atand((V^2)/(r*g)); %[deg]
n = (1/cosd(phi))*1.5;
L_max = n*W; % [lbf]
M_max = 91.47; % [in-lbf] from WingLoad_Distribution Code
M_max_ft = 7.6225; % [ft-lbf]
fiber_comp_safety = fiber_comp/1.5; %[lb/ft^2]
%** I = -M(h/2) / sigma **% [ft] Wolfram Alpha...
%** (.000176 - (1.083 -2*t)*((.125-2*t)^3)/12) = 7.6225*.0625/6.6e6 **%
t = .0025; %[in]

% Failure Bending
M_fail_ft = fiber_comp*(.000176-(1.083-2*t)*((.125-2*t)^3)/12)/(h/2);
M_fail_in = M_fail_ft/12;
%%%%%%%%%%%%%%%%%%%%%%%%%%%%%%%%%%%%%%%%%%%%%%%%%%%%%%%%%%%%%%%%%%%%%%%%
```

The code above implements code that is used, with combination of wolfram alpha, to solve for the required thickness of the fiberglass coating given the flight conditions. Using the bending stress equation, moment of inertia for a hollow rectangular cross section and fiberglass properties a shown below, a required thickness was calculated for maximum bending.

E-Fiberglass Epoxy Properties			
Density [lb/in ³]	Fiber Volume	F _{TU} (L) [psi]	F _{CU} (L) [psi]
0.071	45%	105e3	69e3



$$\sigma = \frac{My}{I_x} \quad I = c * \frac{h^3}{12} - (c - 2t) * \frac{(h - 2t)^3}{12}$$

- Factor of safety: 1.5
- c = 13.5 inches, h = 1.5 inches, $\sigma = 46e3$ psi, M = 91.47 in-lbf
- $I = -M(h/2) / \sigma$
- **t = ~ 0.0004 in**

Using the max twist equation, wing tip angle equation, modulus of rigidity and torsion constant for a hollow rectangular cross section and fiberglass properties, a required thickness was calculated for wing twist. Assumptions for wing twist analysis for fiberglass thickness are listed as follows.

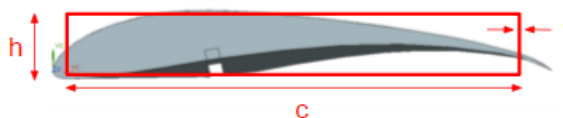
- Only aerodynamic twist
- Skin takes all torsion
- Max twist in sprint
- Wing tip angle $\phi_{\max} < 1^\circ$

The calculated assumptions are:

- $C_m = -0.17$ <http://airfoiltools.com/airfoil/details?airfoil=s1223-il#polars>
- $V_{\max} = 30$ ft / sec

$$T_{\max} = \frac{1}{2} \rho S V_{\max}^2 C_m c \longrightarrow \phi_{\max} = \frac{T_{\max} \frac{b}{2}}{GJ}$$

E-Fiberglass Epoxy Properties			
Density [lb/in ³]	G [psi]	F _{TU} (L) [psi]	F _{CU} (L) [psi]
0.071	0.51e6	105e3	69e3



- G - Modulus of rigidity
- $J = \oint (ds/t) / 4A_0$ (Torsion Constant)

Wing Twist Analysis Values Summary	
rho [slug/in ³]	1.375e-6
S [in ²]	705.6
C _m	-0.17
b [in]	57

- $T_{\max} = -96.48 \text{ in-lbf}$
- $J = 4A_0^2 / \oint (ds/t)$
 - $\oint (ds/t) = 3/t + 26/t$
 - $A_0 = 19.5 \text{ in}^2$
- For $\phi_{\max} = 0.1$
- **$t = \sim 0.0018 \text{ in}$**

Based on the code for the wing load calculations, the failure loading condition for the fiberglass in bending is:

Failure Loading Condition	
Bending	275.25 in-lbf

V-n Diagram Code and Plot

```

%%%%%%%%%%%%%%%%%%%%%%%%%%%%%%%%%%%%%%%%%%%%%%%%%%%%%%%%%%%%%%%%%%%%%%%%
% V-N Diagram Code
% W. Sarmiento
%%%%%%%%%%%%%%%%%%%%%%%%%%%%%%%%%%%%%%%%%%%%%%%%%%%%%%%%%%%%%%%%%%%%%%%%
close all
clear all
clc

% Define the Variables %
m = 4.8;      %lbs
S=4.9;        %ft^2
AR=4.5;
V_c = 27;     %ft/sec
V_d = 27*1.7; %ft/sec
nmax=3.2;
nmin=-1.2;
CLmax= 2.1;
CLmin=1.2;
rho = .0765;  %slugs/ft^3
g = 32.2;     %ft/sec^2
%nmax = V_c^2*rho*S*CLmax/(2*m*g);

% Stall velocity
V_s = sqrt(2*m*g/(rho*S*CLmax)); %ft/sec

% Top Curve
V_nmax = sqrt(m*g*nmax/(0.5*rho*S*CLmax));

% Upper curve equation
n_upperC = 0:.01:nmax;
V_upper = sqrt(m*g*n_upperC./(0.5*rho*S*CLmax));

% Bottom Curve

```

```

V_nmin = sqrt(m*g*nmin/(0.5*rho*S*-CLmin));

% Lower curve equation
n_lowerC = 0:-.01:nmin;
V_lower = sqrt(m*g*n_lowerC./(0.5*rho*S*-CLmin));

% Plotting
plot(V_d,nmin:.01:nmax,'r.') %max speed (vertical line)
hold on
plot(V_nmax:.01:V_d,nmax,'b.') %top line
hold on
plot(V_upper,n_upperC,'b.') %upper curve
hold on
plot(V_nmin:.01:V_d,nmin,'b.') %bottom line
hold on
plot(V_lower,n_lowerC,'b.') %lower curve
axis([0,50,-2,4])
xlabel ('Calibrated Airspeed, ft/sec')
ylabel ('Load Factor, n')
title ('V-n Diagram for Aircraft')
gtext ('Positive Stall Limit')
gtext ('Negative Stall Limit')
gtext ('Positive Structural Limit')
gtext ('Negative Structural Limit')
%%%%%%%%%%%%%%%%%%%%%%%%%%%%%%%%%%%%%%%%%%%%%%%%%%%%%%%%%%%%%%%%%%%%%%%%

```

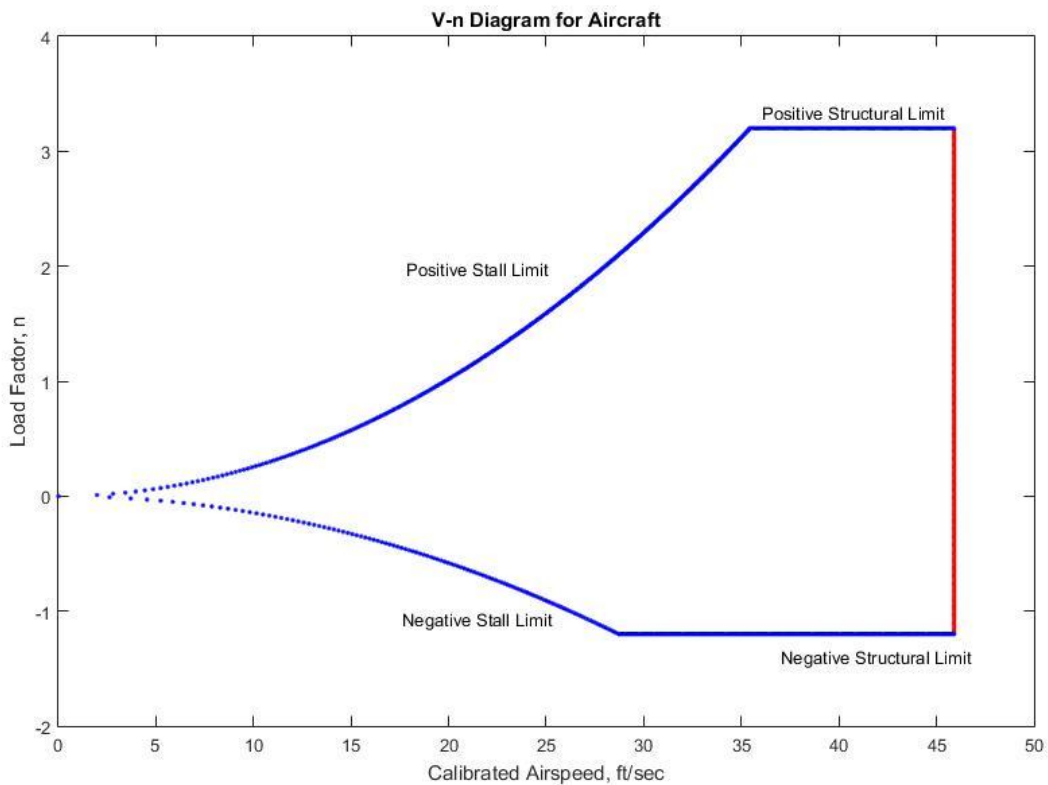


Figure C.3 V-n Diagram

Calculations for Landing Gear Load Analysis

The calculations for the landing gear analysis used a simple implementation of the Euler column equation. The values and equations used for the front landing gear are shown below as follows:

- Load on front gear legs:
 - $F = W \cdot N_{\text{gear}} = \underline{18 \text{ lbf}}$
 - W: total aircraft weight
 - N_{gear} : gear load factor
- Highest compression load of leg from Euler column equation:
 - $P = \pi^2 EI / L^2 = < \underline{916 \text{ lbf}}$

Carbon Fiber Main Gear Properties	
Young's Modulus (E)	1.08e7 [psi]
Moment of Inertia (I) (Cross-Sectional)	.00026 in ⁴
Length (L)	5.5 in

Property Data from Raymer Table 14.3, Pg. 543

The values and equations used for the tail landing gear are shown below as follows:

- Load on tail gear leg:
 - $F = W \cdot N_{\text{gear}} = \underline{9 \text{ lbf}}$
 - W: total aircraft weight
 - N_{gear} : gear load factor
- Highest compression load of leg from Euler column equation:
 - $P = \pi^2 EI / L^2 = < \underline{98.6 \text{ lbf}}$

Nylon Plastic Tail Gear Properties	
Young's Modulus	10e3 [psi]
Moment of Inertia (Cross-Sectional)	.004 in ⁴
Length	2 in

<http://www.curbellplastics.com/>

Appendix D – Dynamics and Stability

Table D.1: Final Dimensions

	Value	Unit
Wing Span	60	inch
Wing Chord	13.5	inch
Aileron Chord	5	inch
Aileron Span	34	inch
Tail Airfoil	NACA0012	-
Horizontal Tail Span	28.5	inch
Horizontal Tail Root Chord	7	inch
Horizontal Tail Tip Chord	5	inch
Vertical Tail Span	11.5	inch
Vertical Tail Root Chord	7	inch
Vertical Tail Tip Chord	5	inch
Elevator Span	26	inch
Rudder Span	10	inch
Elevator Chord	2.5	inch
Rudder Chord	3.5	inch
Vertical Tail Taper Ratio	0.71	-
Horizontal Tail Taper Ratio	0.71	-

Code D.2: X-Plots

```
clc; clear all; close all;
% Xplot for Horizontal Tail
global Sh
Sh = [0:.1:4];
cgfor = 8.71*1.1;
cgaft = 8.71*0.9;
clalphah = 5.73;
clalpha = 5.73;
xbaracw = 0.877;
cmalphaf = 1.10523;
mu = .9;
dalpha = 0.23;
xbarach = 4.3296;
ref = 11.8;

S = 5.01389; %ft^2
% S = 722; %in^2
%roskam vol II pg 261 eq 11.1, 11.2
%F = [1+ (clalphah .* (1 - dehdalpha) .* Sh ./ S) ./clalphawf];
%xbaracA = [.35 + clalphah .* (1 - dehdalpha) .* (Sh/S) * 4.2396] ./
(clalphawf * F);
```



```

delta_cg2=mom_ref_pt-aft_cg;
Cm_aft=+Cl_PlotMax*delta_cg2;
subplot(122);hold on; plot([0 4*Cm_aft],[0 4*Cl_PlotMax],'k') %plot zero line
on CM plot
% str1=['CM about ',num2str(mom_ref_pt),' c'];
xlabel('CM')
ylabel('CL')
title('Trim Diagram by TEAM 3')
grid on
text(.18,.75,['iH= ',num2str(iH),' deg.'])

subplot(121);
z2=axis;
% axis([0 15 0 2.5])
axis([z2(1) 11 0 Cl_PlotMax]);
ylabel('CL')
xlabel('alpha (deg)')
title('Trim Diagram by TEAM 3')
grid on
text2(.1,.95,['iH= ',num2str(iH),' deg.'])
hold off
% Plot alpha_stall line in figure 2
CL=CL0+CLalpha*alpha_stall+CLiH*iH+CLdeltaE*deltaE;
CM=CM0+CMalpha*alpha_stall+CMiH*iH+CMdeltaE*deltaE;
subplot(122); hold on;

plot(CM,CL,'k'); %PLOTS THAT WEIRD LINE
[m,b]=straightline(CM,CL)
hold on
x_var = linspace(-1,1.5)
plot(x_var, m*x_var+b, 'k')
axis([-0.2 0.2 0 2.5])
set(gca, 'XDir', 'reverse'); % reverse the plotting direction on the x axis
% End alpha_stall line plotting

```

Figure D.4: CM Alpha Plot

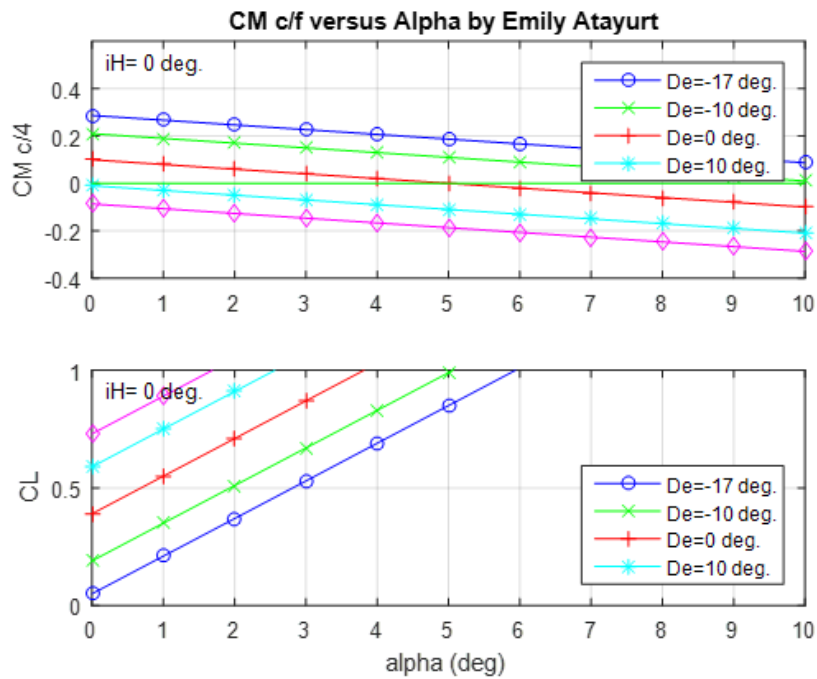
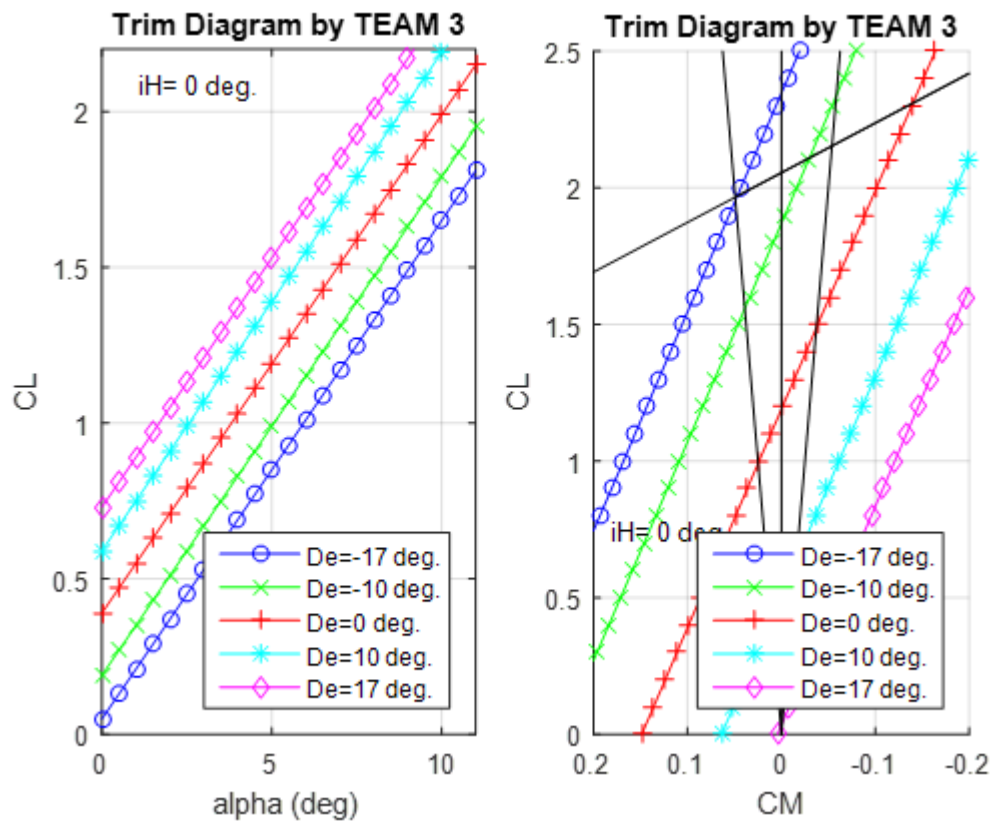


Figure D.5: Trim Diagram



Code D.6: Stability Derivatives

```
%%%%%%%%%%%%%%%%%%%%%%%%%%%%%%%%%%%%%%%%%%%%%%%%%%%%%%%%%%%%%%%%%%%%%%%%%
%Atmospheric Variables
%sea_level_dynamic_pressure = ;
altitude = 300; %ft
%altitude_dynamic_pressure =;
mu_t = 0.9; %assumption
mach_no = 0.2;
beta = sqrt(1-mach_no ^2);
density = 0.034688137; %kg/ft^3
%%%%%%%%%%%%%%%%%%%%%%%%%%%%%%%%%%%%%%%%%%%%%%%%%%%%%%%%%%%%%%%%%%%%%%%%%
%Aircraft variables
wing_root_chord = 13/12; %ft
wing_tip_chord = 10/12; %ft
wingspan = 57/12; %ft
%horizontal tail
h_tail_root_chord = 7/12; %ft
h_tail_tip_chord = 5/12; %ft
h_tail_span = 29/12; %ft
h_tail_arm = 20/12; %ft
%fuselage
fuselage_width = 4.5/12; %ft (bf_max)
fuselage_length = 38/12; %ft (lf)
SB_max = fuselage_width * fuselage_width; %ft^2 (max fuselage cross section)
%Calculated aircraft variables (wing)
S_wing_area = (wing_root_chord * wingspan) - (wing_root_chord -
wing_tip_chord)*4; %ft^2
S_exposed_wing_area = S_wing_area - wing_root_chord * fuselage_width; %ft^2
aspect_ratio = wingspan ^ 2 / S_wing_area; %dimensionless
taper_ratio = wing_tip_chord / wing_root_chord; %ft
mean_aerodynamic_chord = wing_root_chord * 2/3 * ((1 + taper_ratio +
taper_ratio ^ 2) / (1 + taper_ratio));
leading_edge_sweep = atan((wing_root_chord - wing_tip_chord)/2) * pi/180;
%radians
%calculated aircraft variables (horizontal tail)
h_tail_area = (h_tail_root_chord * h_tail_span) - (h_tail_root_chord -
h_tail_tip_chord)*h_tail_span;
horizontal_tail_volume_coeff = (h_tail_area * h_tail_arm) / (S_wing_area *
mean_aerodynamic_chord);
tail_half_chord_sweep = atan((h_tail_root_chord/2 -
h_tail_tip_chord/2)/(h_tail_span/2)) * pi/180; %radians
h_taper_ratio = h_tail_tip_chord / h_tail_root_chord;
h_tail_aspect_ratio = h_tail_span ^ 2 / h_tail_area; %dimensionless
%Flight conditions
theta_0 = 0;
U_0 = 27; %ft/s flight velocity
%Aircraft Characteristics
Cl = .35;
Clalpha = .16;
Cd = 0.048;
Cm = 0.1;
Cmalpha = -0.02;
x_cg = 8.51/12;
x_ac = 12.1/12;
VB = 0.3418; %ft^3
```

```

aircraft_mass = 26.15;    %Newtons
dedalpha = 0.23;
%random matrix components
Iy = 1/12 * aircraft_mass * fuselage_length ^ 2;    %treat as slender rod for
Iy estimate
m1 = 2*aircraft_mass / (density * U_0 * S_wing_area);
c1 = mean_aerodynamic_chord / (2 * U_0);
Iy1 = Iy / (1/2 * density * (U_0) ^ 2 * S_wing_area *
mean_aerodynamic_chord);
%%%%%%%%%%%%%%%%%%%%%%%%%%%%%%%%%%%%%%%%%%%%%%%%%%%%%%%%%%%%%%%%%%%%%%%%
%Stability derivatives
%Clalpha
%->using CFD Clalpha.  However other necessary values will be computed here
K_BW = 0.7890 * (fuselage_length / wingspan) ^ 2 + 1.1976 * (fuselage_length
/ wingspan) + 0.0088;
K_WB = 0.1714 * (fuselage_length / wingspan) ^ 2 + 0.8326 * (fuselage_length
/ wingspan) + 0.9974;
Clalpha_N = 2 * (.92) * SB_max / S_wing_area;
K_N = (Clalpha_N/Clalpha)*(S_wing_area / S_exposed_wing_area);
%%%%%%%%%%%%%%%%%%%%%%%%%%%%%%%%%%%%%%%%%%%%%%%%%%%%%%%%%%%%%%%%%%%%%%%%
%using CFD Cmalpha
%x_ac_wb =
%xbac_ac_wb = x_ac_wb / mean_aerodynamic_chord;
%Cmalpha_WB = (x_cg - xbar_ac_wb) * Clalpha;
%Cmalpha = Cmalpha_WB + Cmalpha_t;
%%%%%%%%%%%%%%%%%%%%%%%%%%%%%%%%%%%%%%%%%%%%%%%%%%%%%%%%%%%%%%%%%%%%%%%%Cdalp****
a1 = 0.0004;
a2 = -0.0080;
a3 = 0.0501;
a4 = 0.8642;
lambda = taper_ratio;
lambda_1 = aspect_ratio * lambda / cos(leading_edge_sweep);    %%%Check here
for error if radian/degree coordination is shitty
R = a1 * lambda_1 ^ 3 + a2 * lambda_1 ^ 2 + a3 * lambda_1 + a4;
oswald = (1.1 * Clalpha) / (R * Clalpha + (1 - R) * pi * aspect_ratio);
k = 1 / (pi * S_wing_area * oswald);
Cdalp = 2 * k * Cl * Clalpha;
%%%%%%%%%%%%%%%%%%%%%%%%%%%%%%%%%%%%%%%%%%%%%%%%%%%%%%%%%%%%%%%%%%%%%%%%Cdu
%low subsonic speeds (M < 0.5), dCd/dM = 0;
Cdu = 0;
%%%%%%%%%%%%%%%%%%%%%%%%%%%%%%%%%%%%%%%%%%%%%%%%%%%%%%%%%%%%%%%%%%%%%%%%Clu
%low subsonic speeds (M < 0.5), dClalpha/dM = 0;
Clu = 0;
%%%%%%%%%%%%%%%%%%%%%%%%%%%%%%%%%%%%%%%%%%%%%%%%%%%%%%%%%%%%%%%%%%%%%%%%Cmu
%low subsonic speeds (M < 0.5), dCmalpha/DmM = 0;
Cmu = 0;
%%%%%%%%%%%%%%%%%%%%%%%%%%%%%%%%%%%%%%%%%%%%%%%%%%%%%%%%%%%%%%%%%%%%%%%%Clq
Clalpha_B = 2 * (.92) * (SB_max / VB ^ (2/3));    %.92 is k2-k1, found by the
fitness ratio and Fig. 3.6 in Pamadi4
Clq_B_prime = Clalpha_B * (VB ^ (2/3) / SB_max);
Clq_B = 2 * Clq_B_prime * (1 - x_cg / fuselage_length);
xi = ((13*.25) - 5.25) / mean_aerodynamic_chord; % xac_e - xcg_le
http://www.nasascale.org/howtos/cg-calculator.htm
Clq_e = (1/2 + 2 * xi)*(Clalpha); %assume Clalpha_e = Clalpha
Clq_wb = (K_WB + K_BW) * (S_exposed_wing_area / S_wing_area) * Clq_e + Clq_B
* (SB_max * fuselage_length / (S_wing_area * mean_aerodynamic_chord));
a_0 = .99;    %from data sheets

```

```

k_a_t = a_0 / (2*pi);
a_t = (2*pi*h_tail_area) / (2 + sqrt(((h_tail_area ^ 2) * beta ^ 2) / (k_a_t
^ 2))) * (1 + tan(tail_half_chord_sweep)^2/beta^2 + 4));
Clq_t = 2 * a_t * horizontal_tail_volume_coeff * mu_t;
Clq = Clq_wb + Clq_t;
%%Cmq
x0 = 6.3/12;
Cmalpha_B = 2 * (.92) / VB * (SB_max * (x_cg - x0));
Cmalpha_B_prime = Cmalpha_B * (VB / (fuselage_length * SB_max));
xc = 8.57/12; %complicated integral - just estimating a value
V_b1 = VB / (fuselage_length * SB_max);
xc1 = xc / fuselage_length;
xm1 = x_cg / fuselage_length;
Cmq_B = 2 * Cmalpha_B_prime * (((1-xm1)^2 - V_b1 * (xc1 - xm1))/(1 - xm1 -
V_b1));
B = sqrt(1 - mach_no^2 * cos(leading_edge_sweep)^2);
c5 = aspect_ratio + 2 * cos(leading_edge_sweep);
c4 = aspect_ratio + 6 * cos(leading_edge_sweep);
c3 = aspect_ratio*B + 6 * cos(leading_edge_sweep);
c2 = 3 / B;
cla = aspect_ratio ^ 3 * tan(leading_edge_sweep)^2;
Cmq_e_M = -0.7 * Clalpha * cos(leading_edge_sweep)*((aspect_ratio * 0.5*xi +
2 * xi ^ 2)/c5 + (cla/24*c4) + 1/8);
Cmq_e = ((cla/c3 + c2)/(cla/c4 + 3))*Cmq_e_M;
Cmq_WB = (K_WB + K_BW) * (S_exposed_wing_area / S_wing_area) * Cmq_e + Cmq_B
* SB_max / S_wing_area * (fuselage_length / mean_aerodynamic_chord)^2;
Cmq_t = - 2 * a_t * horizontal_tail_volume_coeff * mu_t *
(h_tail_arm/mean_aerodynamic_chord);
Cmq = Cmq_WB + Cmq_t;
%Clalphadot
Clalpha_B = 2 * (.92) * SB_max / (VB ^ (2/3));
Clalpha_B_prime = Clalpha_B * (VB ^ (2/3) / (SB_max * fuselage_length));
Clalphadot_B = 2 * Clalpha_B_prime * (VB / (SB_max * fuselage_length));
tau = beta * aspect_ratio;
Cl_g = ((-pi * aspect_ratio) / (2 * beta ^ 2)) * (0.0013*tau^4 - 0.0122*tau^3
+ 0.0317*tau^2 + 0.0186*tau - 0.0004);
Clalphadot_e = 1.5 * (x_ac / wing_root_chord) * Clalpha + 3 * Cl_g;
Clalphadot_WB = (K_WB + K_BW) * (S_exposed_wing_area / S_wing_area) *
Clalphadot_e + Clalphadot_B * ((SB_max * fuselage_length) / (S_wing_area *
mean_aerodynamic_chord));
Clalphadot_t = 2 * a_t * horizontal_tail_volume_coeff * mu_t * dedalpha;
Clalphadot = (Clalphadot_WB) + Clalphadot_t;
%Cmalphadot
Cmalphadot_B = 2 * (Cmalpha_B_prime) * ((xc1 - xm1) / (1 - xm1 - V_b1))*(VB /
(SB_max * fuselage_length));
Cm0_g = ((pi*aspect_ratio)/(2*beta^2))*(.0008*tau^4 - .0075*tau^3
+0.0185*tau^2 + 0.0128*tau - 0.0003);
Cmalpha_e_doubleprime = -(81/32)*(x_ac/wing_root_chord)^2 * Clalpha + 9/2 *
Cm0_g;
Cmalpha_e = Cmalpha_e_doubleprime +
(5.25/mean_aerodynamic_chord)*(Clalphadot_e);
Cmalphadot_WB = (K_WB + K_BW) * (S_exposed_wing_area / S_wing_area) *
Cmalpha_e + Cmalpha_B * ((SB_max * fuselage_length ^ 2) / (S_wing_area *
(mean_aerodynamic_chord)^2));
Cmalphadot_t = -2 * a_t * horizontal_tail_volume_coeff * mu_t * (dedalpha) *
(h_tail_arm / mean_aerodynamic_chord);
Cmalphadot = Cmalphadot_WB + Cmalphadot_t;

```



```

%Matrix Component Components ??
Cxu = -2 * Cd - Cdu;
Cxalpha = Cl - Cdalpaha;
Cxtheta = -Cl * cos(theta_0);
Cxalphadot = 0; % -Cdalphadot; %USUALLY 0
Cxq = 0; %-Cdq; %USUALLY 0
Czu = -2 * Cl - Clu;
Czalpaha = -Clalpha - Cd;
Czalphadot = -Clalphadot;
Czq = -Clq;
Cztheta = -Cl * sin(theta_0);
xi_1 = Cxalphadot * c1 / (m1 - Czalphadot*c1);
xi_2 = Cmalphadot * c1 / (m1 - Czalphadot * c1);
%%%%%%%%%%%%%%%%%%%%%%%%%%%%%%%%%%%%%%%%%%%%%%%%%%%%%%%%%%%%%%%%%%%%%%%%
%A matrix components
a_11= (Cxu + xi_1 * Czu) / m1;
a_12= (Cxalpha + xi_1 * Czalpaha) / m1;
a_13= (Cxq * c1 + xi_1 * (m1 + Czq * c1)) / m1;
a_14= (Cxtheta + xi_1 * Cztheta) / m1;
a_21= Czu / (m1 - Czalphadot * c1);
a_22= Czalpaha / (m1 - Czalphadot * c1);
a_23= (m1 + Czq * c1) / (m1 - Czalphadot * c1);
a_24= Cztheta / (m1 - c1 * Czalphadot);
a_31= (Cmu + xi_2 * Czu) / Iy1;
a_32= (Cmalpaha + xi_2 * Czalpaha) / Iy1;
a_33= (Cmq * c1 + xi_2 * (m1 + Czq * c1)) / Iy1;
a_34= xi_2 * Cztheta / Iy1;
a_41= 0;
a_42= 0;
a_43= 1;
a_44= 0;
%B matrix components
%b_1 = (Cxdeltae + xi_1 * Czdeltae) / m1;
%b_2 = Czdeltae / (m1 - c1 * Czalphadot);
%b_3 = (Cmdeltae + xi_2 * Czdeltae) / Iy1;
%b_4 = 0;
%A matrix
A = [a_11 a_12 a_13 a_14; a_21 a_22 a_23 a_24; a_31 a_32 a_33 a_34; a_41 a_42
a_43 a_44];
%B matrix
%B_matrix = [b_1; b_2; b_3; b_4];
%C matrix
%%%%%%%%%%%%%%%%%%%%%%%%%%%%%%%%%%%%%%%%%%%%%%%%%%%%%%%%%%%%%%%%%%%%%%%%Short period matrix
d_11 = Czalpaha / (m1 - Czalphadot*c1);
d_12 = (m1 + Czq * c1) / (m1 - Czalphadot*c1);
d_21 = (1/Iy1)*(Cmalpaha + (Cmalphadot * c1 * Czalpaha)/(m1 - Czalphadot *
c1));
d_22 = (1/Iy1)*(Cmq * c1 + (Cmalphadot * c1 / (m1 - Czalphadot * c1)) * (m1 +
c1 * Czq));
D_sp = [d_11 d_12; d_21 d_22];
short_period_natural_frequency = sqrt((Czalpaha*c1*Cmq)/(m1*Iy1) -
Cmalpaha/Iy1);
short_period_damping_ratio = -(Czalpaha/m1 + (c1/Iy1)*(Cmq +
Cmalphadot))/(2*short_period_natural_frequency);
%phugoid
phugoid_natural_frequency = 1/m1 * sqrt(-Cl * -2*Cl);
phugoid_damping_ratio = -Czu / (2*m1*phugoid_natural_frequency);

```

```

% 747 longitudinal axis example for 263
% 40000 feet steady, level flight, 774 ft/sec
% from bryson p151
% x = u, w, q, theta
%A = [ -0.003 0.039 0 -0.322; -0.065 -0.319 7.74 0; 0.020 -0.101 -0.429 0; 0 0 1
0];
%input = u_w, w_w, delta_e, delta_t
Bw= -A(:, [1,2]); Bc= [0.01 1; -0.18 -0.04; -1.16 .598; 0 0]; B = [Bw,Bc];
% output: u, climb rate = -w + 7.74 theta
C = [ 1 0 0 0; 0 -1 0 7.74];
H0 = -C*inv(A)*B;
H01 = H0(:, [3,4]); % DC gain matrix from delta_e delta_t to
% speed, climb rate
% modal analysis
[V,Gam]=eig(A); xshort = real(V(:,1)); xphug = real(V(:,3));
xshort = xshort/norm(xshort); xphug = xphug/norm(xphug);
Nsamp = 100; %number of time samples
yshort=zeros(2,Nsamp); t=linspace(0,20,Nsamp);
for i=1:Nsamp;
    yshort(:,i)=C*expm(t(i)*A)*xshort;
end
figure(3)
subplot(2,1,1)
plot(t,yshort(1,:));
axis([0 20 -1 1])
ylabel('aircraft velocity (ft/s)')
title('short period mode response');
subplot(2,1,2)
plot(t,yshort(2,:));
axis([0 20 -1 1])
ylabel('climb rate (ft/s)')
xlabel('time (seconds)')
print -deps aircraft_short
Nsamp = 400; %number of time samples
yshort=zeros(2,Nsamp); t=linspace(0,2000,Nsamp);
for i=1:Nsamp;
    yphug(:,i)=C*expm(t(i)*A)*xphug;
end
figure(4)
subplot(2,1,1)
plot(t,yphug(1,:));
axis([0 2000 -2 2])
ylabel('aircraft velocity (ft/s)')
title('phugoid mode response');
subplot(2,1,2)
plot(t,yphug(2,:));
axis([0 2000 -2 2])
ylabel('climb rate (ft/s)')
xlabel('time (seconds)')
print -deps aircraft_phug

```

Table D.7 - Aerodynamic Center Calculation

The aerodynamic center is first calculated by relating the static margin to the aerodynamic center, then the static margin relation to the moment and lift coefficients. This is shown in the following equations:

$$SM = -CMCL$$

$$SM = (x_{np} - x_{cg})/c$$

$$-CMCL = (x_{np} - x_{cg})/c$$

$$C_m = C_{Lw}x_{ACw} + C_{Lh}X_{ACh}q_h S(1 - dd)$$

By defining all the preceding variables, we can calculate the static margin and the location of the aerodynamic center of the aircraft.

C _m	Moment Coefficient	-moment generated about the aircraft	unknown
C _{Lw}	Lift Coefficient of Wing	-lift coefficient for the wing of the aircraft	5.73 (deg/rad)
x _{ACw}	Aerodynamic Center of Wing + Fuselage	-the distance of the aerodynamic center of the wing and fuselage from the center of gravity of the aircraft, with respect to mean aerodynamic center	0.105 (non-dimensionalized)
C _{Lh}	Lift Coefficient of Horizontal Tail	-lift coefficient for the tail of the aircraft	5.73 (deg/rad)
X _{ACh}	Aerodynamic Center of Horizontal Tail	-distance of the aerodynamic center of the wing from the center of gravity with respect to mean aerodynamic center	2.027634628 (non-dimensionalized)
q _h	Dynamic Pressure (h)	-dynamic pressure around horizontal tail	9 (assumed as ratio)
q	Dynamic Pressure	-dynamic pressure about wing	10 (assumed as ratio)
S _h	Area of Horizontal Tail	-square inch area of tail	171 (square inches)
S	Area of Wing	-square inch area of wing	705.63 (square inches)
dd	Downwash Coefficient	-effect of downwash on horizontal tail	0.23

c	M.A.C.	-mean aerodynamic chord of wing	11.565 (inches)
---	--------	---------------------------------	-----------------

Therefore,

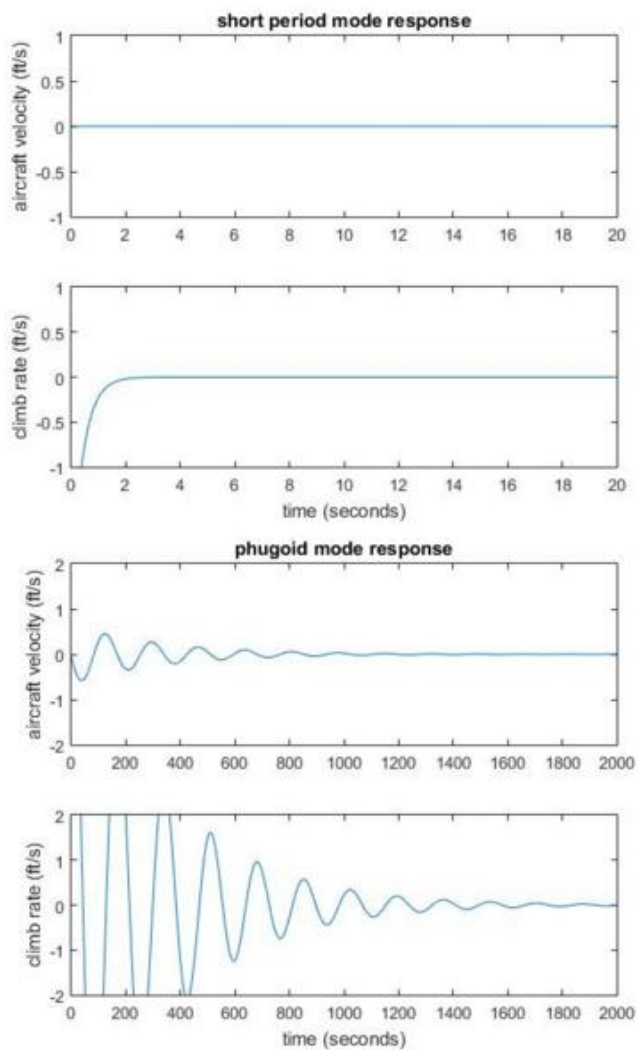
$$SM = [(-1) * (5.73 \text{ deg/rad})(0.105) - (5.73 \text{ deg/rad})(2.0276)(.9)(171 \text{ in}^2 / 705.63 \text{ in}^2)(1 - 0.23)] / (5.37 \text{ deg/rad})$$

$$SM = 0.2426 = (x_{np} - x_{cg}) / c$$

$$0.2426 = (x_{np} - 9.3) / 11.565$$

$$x_{np} = 12.105 \text{ inches}$$

Figure D.8 - Mode Graphical Analysis



Appendix E – Sense and Avoid



Figure D.1: The LIDAR device

Dimensions: 21 x 48.3 x 35.5 mm

Features:

- Range: 0-40m Laser Emitter
- Accuracy: +/- 0.025m
- Power: 5V DC
- Current Consumption: <100mA continuous operation
- Acquisition Time: < 0.02 sec
- Rep Rate: 1-500Hz
- Interface: I²C or PWM
- Weight: 0.04lbs

All of this data was taken from the website Sparkfun⁸.

“LIDAR Lite 2”. Sparkfun. Retrived

from: <https://www.sparkfun.com/products/13680?gclid=CPPvjM6Hs8gCFQkxaQod2SsNxA>

Appendix F – Economics

Table F.1: Budget Details

Item	Price	Quantity	Total	Shipping Cost
<i>Foam</i>	<i>\$26.00</i>	<i>1</i>	<i>\$26.00</i>	<i>\$0.00</i>
<i>Carbon Fiber Rod Outer</i>	<i>\$8.00</i>	<i>2</i>	<i>\$16.00</i>	<i>\$0.00</i>
<i>Carbon Fiber Rod Inner</i>	<i>\$12.00</i>	<i>1</i>	<i>\$12.00</i>	<i>\$0.00</i>
<i>LIDAR-Lite</i>	<i>\$114.89</i>	<i>1</i>	<i>\$114.89</i>	<i>\$0.00</i>
<i>Camera</i>	<i>\$16.99</i>	<i>1</i>	<i>\$16.99</i>	<i>\$0.00</i>
<i>Rasbery Pi B</i>	<i>\$38.85</i>	<i>1</i>	<i>\$38.85</i>	<i>\$0.00</i>
<i>Landing Gear Front Wheels</i>	<i>\$10.44</i>	<i>1</i>	<i>\$10.44</i>	<i>\$0.00</i>
<i>Landing Gear Back Wheels</i>	<i>\$4.80</i>	<i>1</i>	<i>\$4.80</i>	<i>\$0.00</i>
<i>Battery</i>	<i>\$28.93</i>	<i>1</i>	<i>\$28.93</i>	<i>\$0.00</i>
<i>Motor</i>	<i>\$15.98</i>	<i>1</i>	<i>\$15.98</i>	<i>\$0.00</i>
<i>Speed Controller</i>	<i>\$13.30</i>	<i>1</i>	<i>\$13.30</i>	<i>\$0.00</i>
<i>Extra Gear</i>	<i>\$5.89</i>	<i>1</i>	<i>\$5.89</i>	<i>\$0.00</i>
<i>Gearbox</i>	<i>\$17.98</i>	<i>1</i>	<i>\$17.98</i>	<i>\$0.00</i>
<i>Propellers</i>	<i>\$5.00</i>	<i>1</i>	<i>\$5.00</i>	<i>\$0.00</i>
<i>Neodymium Magnets</i>	<i>\$8.99</i>	<i>1</i>	<i>\$8.99</i>	<i>\$0.00</i>
<i>Balsa Wood Sheets</i>	<i>\$4.27</i>	<i>1</i>	<i>\$4.27</i>	<i>\$2.95</i>
<i>servos</i>	<i>\$10.73</i>	<i>4</i>	<i>\$42.92</i>	<i>\$0.00</i>
<i>servo rods</i>	<i>\$2.27</i>	<i>2</i>	<i>\$4.54</i>	<i>\$0.00</i>
<i>Servo Horns</i>	<i>\$1.22</i>	<i>2</i>	<i>\$2.44</i>	<i>\$0.00</i>
<i>wheel for landing gear</i>	<i>\$5.85</i>	<i>1</i>	<i>\$5.85</i>	<i>\$3.99</i>
<i>landing gear axle</i>	<i>\$6.39</i>	<i>1</i>	<i>\$6.39</i>	<i>\$0.00</i>
<i>Signal to Pilot WiFi</i>	<i>\$5.95</i>	<i>1</i>	<i>\$5.95</i>	<i>\$0.00</i>
SUM:			\$408.40	\$6.94

Figure F.2: Scheduling Part 1


97		✦ Build Process	21 days	Thu 10/22/15	Thu 11/19/15	
98		Place ALL orders	2 days	Thu 10/22/15	Fri 10/23/15	66
99		✦ Wing	9 days	Thu 10/22/15	Tue 11/3/15	
100		Carbonfiber rods delivered	4 days	Mon 10/26/15	Thu 10/29/15	98
101		Hotwire wing sections	1 day	Thu 10/22/15	Thu 10/22/15	66
102		Fiberglass wing	2 days	Fri 10/23/15	Mon 10/26/15	101
103		Magnets delivered	5 days	Mon 10/26/15	Fri 10/30/15	98
104		Glue wing sections	2 days	Tue 10/27/15	Wed 10/28/15	102
105		Check attachability	0.5 days	Thu 10/29/15	Thu 10/29/15	104
106		Check fit in box	0.5 days	Thu 10/29/15	Thu 10/29/15	105
107		Install magnets	2 days	Mon 11/2/15	Tue 11/3/15	106,103
108		✦ Tail	11 days	Thu 10/22/15	Thu 11/5/15	
109		Hotwire tail sections	1 day	Thu 10/22/15	Thu 10/22/15	66
110		Fiberglass tail	2 days	Fri 10/23/15	Mon 10/26/15	109
111		Check attachability	0.5 days	Tue 10/27/15	Tue 10/27/15	110
112		Check fit in box	0.5 days	Tue 10/27/15	Tue 10/27/15	111
113		Determine appropriate servo horn attachment location	3 days	Tue 11/3/15	Thu 11/5/15	111,136
114		✦ Fuselage	10 days	Thu 10/22/15	Wed 11/4/15	
115		Cut foam board	2 days	Thu 10/22/15	Fri 10/23/15	66
116		Sand foam board	2 days	Mon 10/26/15	Tue 10/27/15	115
117		Tape fuselage	2 days	Wed 10/28/15	Thu 10/29/15	116
118		Cut tail attachment	1 day	Fri 10/30/15	Fri 10/30/15	117
119		Cut wing attachment	1 day	Fri 10/30/15	Fri 10/30/15	117
120		Check attachability	0.5 days	Mon 11/2/15	Mon 11/2/15	118,119
121		Check fit in box	0.5 days	Mon 11/2/15	Mon 11/2/15	120
122		Insert Velcro for electronics	2 days	Tue 11/3/15	Wed 11/4/15	121
123		▷ Propulsion	16 days	Mon 10/26/15	Mon 11/16/15	
128		▷ Sense and Avoid	18 days	Mon 10/26/15	Wed 11/18/15	
135		▷ Control System/Electronics	19 days	Mon 10/26/15	Thu 11/19/15	
139		Due	0 days	Thu 11/19/15	Thu 11/19/15	

Figure F.2: Scheduling Part 2

97		▣ Build Process	21 days	Thu 10/22/15	Thu 11/19/15	
98		Place ALL orders	2 days	Thu 10/22/15	Fri 10/23/15	66
99		▷ Wing	9 days	Thu 10/22/15	Tue 11/3/15	
108		▷ Tail	11 days	Thu 10/22/15	Thu 11/5/15	
114		▷ Fuselage	10 days	Thu 10/22/15	Wed 11/4/15	
123		▣ Propulsion	16 days	Mon 10/26/15	Mon 11/16/15	
124		Electronics delivered	14 days	Mon 10/26/15	Thu 11/12/15	98
125		Static test for battery life	2 days	Fri 11/13/15	Mon 11/16/15	124
126		Attach electronics in fuselage	1 day	Thu 11/5/15	Thu 11/5/15	122,136
127		Check CG	1 day	Fri 11/6/15	Fri 11/6/15	126
128		▣ Sense and Avoid	18 days	Mon 10/26/15	Wed 11/18/15	
129		Sensors delivered	10 days	Mon 10/26/15	Fri 11/6/15	98
130		Generate code for sensors	12 days	Mon 10/26/15	Tue 11/10/15	129SS
131		Static test on ground for sensors	2 days	Wed 11/11/15	Thu 11/12/15	130,122
132		Dynamic test on ground for sensors	2 days	Fri 11/13/15	Mon 11/16/15	131
133		Attach electronics on wings	1 day	Tue 11/17/15	Tue 11/17/15	107,132
134		Complete wiring	1 day	Wed 11/18/15	Wed 11/18/15	133
135		▣ Control System/Electronics	19 days	Mon 10/26/15	Thu 11/19/15	
136		Servos delivered	6 days	Mon 10/26/15	Mon 11/2/15	98
137		Perform system checks	0.5 days	Thu 11/19/15	Thu 11/19/15	136,122,126,134,113,107
138		Install wiring (servo, motor, battery, receiver, Arduino)	0.5 days	Thu 11/19/15	Thu 11/19/15	137
139	📅	Due	0 days	Thu 11/19/15	Thu 11/19/15	

List F.3: Flight Test Plan

- To be performed inside:
 - Check that all components fit in box
 - Structural integrity (i.e. nothing falls off)
 - Check that all servos function individually
 - Check engine start
 - Battery endurance test
 - Perform ground sense and avoid test
- To be performed outside:
 - Check that signals are transmitting on the ground from a range of 300 - 400 ft
- To be performed flight (outside):
 - Perform glide test with trim deflections
 - Sensing test with sense and avoid equipment

Risk: Team plans to build two complete models, so the risk is low.